

To appear in Ap.J.

# Near Infrared Spectroscopic Monitoring of EXor variables: First Results <sup>1</sup>

D.Lorenzetti<sup>2</sup> V.M.Larionov<sup>3,4</sup>, T.Giannini<sup>2</sup>, A.A.Arkharov<sup>4</sup>, S.Antoniucci<sup>2</sup>, B.Nisini<sup>2</sup>, and  
A.Di Paola<sup>2</sup>

Received;Accepted

## ABSTRACT

We present low resolution ( $\mathcal{R} \sim 250$ ) spectroscopy in the near-IR (0.8 to 2.5  $\mu\text{m}$ ) of the EXor variables. These are the initial results (obtained during the period 2007-2008) from a long term photometric and spectroscopic program aimed to study the variability in the accretion processes of pre-Main Sequence (PMS) stars, by correlating the continuum fluctuations with the spectroscopical properties. Eight sources have been observed in different epochs, for a total of 25 acquired spectra. EXor spectra show a wide variety of emission features dominated by HI recombination (Paschen and Brackett series). We have investigated whether line and continuum variability could be due to a variable extinction, but such hypothesis is applicable only to the peculiar source PV Cep. By comparing the observed spectra with a wind model, mass loss rates in the range  $(2-10) 10^{-8} \text{ M}_{\odot} \text{ yr}^{-1}$  are derived, along with other wind parameters. Consistent results are also obtained by assuming that HI lines are due to accretion. CO overtone is also detected in the majority of the sources both in absorption and in emission. It appears to come from regions more compact than winds, likely the stellar photosphere (when in absorption) and the circumstellar disk (when in emission). NaI and CaI IR lines behave as the CO does, thus they are thought to arise in the same locations. For some targets multiple spectra correspond to different activity stages of the source. Those exhibiting the largest continuum variation

---

<sup>2</sup>INAF - Osservatorio Astronomico di Roma, via Frascati 33,I-00040 Monte Porzio, Italy, dloren, giannini, antoniucci, nisini, dipaola, dloren@oa-roma.inaf.it

<sup>3</sup>Astronomical Institute of St.Petersburg University, Russia, vlar@nm.ru

<sup>4</sup>Central Astronomical Observatory of Pulkovo, Pulkovskoe shosse 65, 196140 St.Petersburg, Russia, arkharov@mail.ru

at  $2\ \mu\text{m}$  ( $\Delta K \gtrsim 1\ \text{mag}$ ) present a significant line flux fading during the continuum declining phases. In particular, CO absorption (emission) appears associated to inactive (active) stages, respectively.

*Subject headings:* circumstellar matter – infrared: stars – stars: emission-line – stars: formation – stars: pre-main sequence – stars: variables: EXor

## 1. Introduction

EXor stars, originally defined by Herbig (1989), are Pre-Main Sequence objects, with ages of about  $10^6$  years, characterized by intense (3-4 magnitudes) and short living (months, one year) outbursts superposed to longer (some years) quiescence periods. According to a widely accepted picture, such objects are accreting material from a circumstellar disk, through rapid and intermittent accretion events that generate thermal instabilities in the disk itself and, eventually, outbursts phenomena (Hartmann & Kenyon 1985). Indeed the accreted matter migrates toward the central star and it is suddenly halted where the inner disk is truncated (at few stellar radii) by the dipolar stellar magnetic field; then it is channelled onto the stellar surface along the magnetic field lines (e.g. Shu et al. 1994). When such material violently falls onto the stellar surface produces a shock that cools by emitting a hot continuum, often called veiling. As a consequence of the accretion event, strong winds (in some cases also collimated jets) emerge from the rotating star/disk system. While the accretion phenomenology is difficult to be directly observed, the observations of young objects more likely reveal the presence of outflowing matter whose rate is often exploited to quantitatively determine the rate of the infalling one, by invoking the rough proportion  $\dot{M}_{wind}/\dot{M}_{acc} \lesssim 0.1$  (Shu et al. 2000; Königl & Pudritz 2000).

The interaction with a close binary companion is also invoked as an alternative mechanism to produce accretion disk instabilities and consequent outbursts (Clarke, Lin & Pringle 1990; Bonnell & Bastien 1992). Indeed, the majority of EXor do have a close companion which could trigger the flares when it passes at the periastron. A suggestion in this sense has been provided to account for the rapid variations of UZ Tau E (Jensen et al. 2007), and an increasing number of observational studies are currently oriented in such direction. However, extending the close companion interpretation to the whole class has not proved to be able

---

<sup>1</sup>Based on observations collected at the AZT-24 telescope (Campo Imperatore, Italy)

to explain the complex phenomenology (e.g. the timescale variability) observed in EXor’s. The present paper focusses on the correlations between continuum and lines variability, be they intrinsic to the source or triggered by the external environment. Continuum and line observations at different frequencies trace phenomena that occur in completely different regions of these complex systems (from the outer disk to the stellar surface and even in the external envelope and in the chromosphere). Although the flaring-up events represent a very important phase of the Pre-Main Sequence life, the continuum and spectral line variability are rarely correlated and very few spectroscopic studies exist to date that compare outburst vs quiescence observational properties. Herbig (2007) provides an optical monitoring of EX Lup (the prototype of the EXor class) which covers a long period during which four subsequent flareups occurred. The spectroscopic consequences of the outburst are the appearance of both a hot continuum and an emission line structure where inverse P Cyg absorption features are superposed. Five EXor candidates (NY Ori, V1118 Ori, V1134 Ori, V1184 Tau, and V350 Cep) have been compared both photometrically and spectroscopically with EX Lup, looking for common features (Herbig 2008). Spectroscopical monitoring studies in the visual band have been presented for other EXor’s, namely DR Tau (Beristain et al. 1998), VY Tau (Herbig 1990), PV Cep (Cohen et al. 1981). Typically, when the star is inactive the spectrum shows absorption features of a M0 star, while a remarkable emission spectrum appears during the active phases. Similar studies in the IR band are still missing, although they should be crucial during both inactive and active phases: in the former stages they allow us to investigate how the properties of the circumstellar matter prior the outburst will influence, through the accretion, the outburst itself; while, in the latter stages the IR spectroscopy is a suitable tool to sample how the circumstellar material is altered by intermittent mass loss. In this wavelength range, the only monitored variation is a decrease of the line emission intensity by more than a factor of six detected in the near IR spectrum of the EXor V1118 Ori, passing from active to inactive status (Lorenzetti et al. 2007, hereinafter Paper II).

Quite recently different outbursting and fading phases of another young object, i.e. V1647 Ori, have been spectroscopically monitored in IR (Gibb et al. 2006; Acosta-Pulido et al. 2007) demonstrating how the post-outburst phase is characterized by a declining temperature of the hot CO gas formed in the inner part of the disk, and by a substantial decrease of the fast wind. In particular, after one year of quiescence, HI and He recombination are decreased by one order of magnitude and CO lines appear in absorption instead of in emission (Aspin, Beck & Reipurth 2008). These latter authors argue in favour of the membership of this embedded object to the EXor class (instead to the FUor one), since its recent activity lasted only two years and 40 years ago it was observed in outburst. Near-IR

spectra have been provided for the embedded variable OO Ser (Hodapp 1999; Kóspál et al. 2007), but, again, some doubts on its attribution to the EXor class have been risen by the authors themselves by invoking both the wavelength-independence of the fading and the variability timescales. A somehow unified interpretative scheme able to account for the observed near-IR spectra of EXor, does not exist, at the moment. To understand the correlation between the gas properties due to accretion/ejection activity and the continuum variation in the near-IR, we have started a spectroscopical monitoring program in the range 0.8-2.5  $\mu\text{m}$ , and the first results are presented here. Our scope is also to ascertain whether or not the conclusions mentioned above for individual objects can be ascribed to the whole EXor class and to examine the similarities vs. differences that characterize their near-IR spectra.

In Paper II the IR (1-100  $\mu\text{m}$ ) photometric properties of the EXor have been discussed, while in the present paper more emphasis is given to the spectroscopic properties and to their correlations with the continuum status. For some targets, those presented here represent the first IR spectra ever taken, hence this paper aims hopefully to contribute in creating an initial data-base for future comparison purposes. After having defined the EXors sample and provided the details of our observations in Sect.2, we present in Sect.3 our spectroscopic results. In Sect.4 these are interpreted by means of a wind model to derive the physical properties of the emitting gas; our concluding remarks are given in Sect.5.

## 2. Observations

The list of the investigated targets is given in Table 1 along with some relevant parameters. The tenth column indicates whether or not a close companion has been found, providing in the affirmative cases the inter-distance in arcsec. Our list is essentially the one originally provided by Herbig (1989), where EX Lup is missing because of its southern location inaccessible by our instrumentation.

Near-IR data were obtained at the 1.1m AZT-24 telescope located at Campo Imperatore (L'Aquila - Italy) equipped with the imager/spectrometer SWIRCAM (D'Alessio et al. 2000), which is based on a 256 $\times$ 256 HgCdTe PICNIC array. Low resolution ( $\mathcal{R} \sim 250$ ) spectroscopy is obtained by means of two IR grisms  $G_{blue}$  and  $G_{red}$  covering the ZJ (0.83 - 1.34  $\mu\text{m}$ ) and HK (1.44 - 2.35  $\mu\text{m}$ ) bands, respectively, in two subsequent exposures. The long slit is not orientable in position angle, and it samples a pre-defined portion of the focal plane, 2 $\times$ 260 arcsec<sup>2</sup> in the east-west direction.

Long-slit spectroscopy was carried out in the standard ABB'A' mode with a total inte-

gration time ranging between 800 and 1200 sec. In Table 2 the Log of our observations is given. The spectral images were flat-fielded, sky-subtracted, and corrected for the optical distortion in both the spatial and spectral directions. The object spectra were corrected for the atmospheric spectral response dividing them by the spectrum of a telluric O-type star, having normalized this latter for the black-body spectrum at the stellar temperature and replaced its intrinsic hydrogen absorption lines with the black-body function at the same wavelengths. Wavelength calibration was derived from the OH lines present in the raw spectral images, while flux calibration was obtained from our photometric data taken to implement our database on IR observations of EXors.

Such photometry, carried out on the same night of the spectroscopy, is given in Table 2 in form of J,H and K magnitudes, provides an indication of the current brightness status of the source compared with the historical behavior derived from the literature (see Paper II). The same Table 2 is complemented with information about the spectroscopic observations in the near IR (1-2.5  $\mu\text{m}$ ) available in the literature.

### 3. Results

The results given here represent the first survey of EXors spectra carried out in a systematic way, namely by observing a complete sample with the same equipment and by adopting the same observational modalities and reduction techniques. For two objects (NY Ori and V1143 Ori) these represent the first near-IR spectra ever obtained. In the following, the EXor source V1118 Ori will be incorporated in the discussion, although its spectroscopic data have been already presented elsewhere (Papers I and II). The calibrated spectra are given in Figures from 1 to 7 and the derived unreddened line fluxes in Tables from 3 to 9. The lines showing a S/N ratio between 2 and 3 are still listed in the Tables and marked with an asterisk, but they are not considered in the following analysis. In the same Tables, for any line flux the equivalent width (EW) is given, as well. The EW does not represent a straightforward spectral diagnostic, since it crucially depends on the continuum level; however, since their values vary significantly, EW's are signalling that spectroscopical variations do not merely follow the continuum ones.

At our sensitivity and at the epoch of our survey, some objects appear as emission lines rich (UZ Tau, DR Tau, V1118 Ori and PV Cep), other (XZ Tau, VY Tau, NY Ori and V1143 Ori) present just few features, usually in emission: these are plausibly the brightest lines of a spectrum weaker, but intrinsically composed by the same features present in the line rich objects. These latter spectra are dominated by hydrogen recombination (Brackett and Paschen series) which signals the presence of ionized gas close to the star. In all the

spectra  $\text{Pa}\beta$  is detected as a broad feature at the corresponding wavelength: at  $\mathcal{R} \sim 250$ , this typical feature may be due to the closeness of  $\text{Pa}\beta$  and  $\text{HeI}$  at  $1.285 \mu\text{m}$ , however, because of its relative faintness, the latter cannot be confidently resolved.

The CO overtone features  $v=2-0$ ,  $v=3-1$  (both in emission and absorption) are clearly detected in the majority of cases (7 out of 8); the same occurs in several young stellar objects (Carr 1989), at variance with the majority of the FUor where CO bands are revealed always in absorption (Hartmann, Hinkle & Calvet 2004). The CO features are highly variable on relatively short (some months) timescales. Besides CO flux variations, during our monitoring period the CO bands have been observed even to change from emission to absorption (DR Tau, V1118 Ori and NY Ori). Such a behaviour is quite typical of low luminosity young stellar objects, as monitored by Biscaya et al. (1997).

Atomic features of both NaI at  $2.208 \mu\text{m}$  and, more rarely, CaI at  $2.267 \mu\text{m}$ , are also detected: in emission in those cases of CO emission, and in absorption when also CO occurs in absorption. This circumstance suggests the presence of a common origin for Na, Ca and CO transitions; this topic will be discussed in Sect.4.5. We note that a NaI line has been also detected, in absorption (Herbig et al. 2001), in the near-IR spectrum of EX Lup, the prototype of the EXor class. Molecular hydrogen and ionized iron emission are absent at our sensitivity level in all the spectra indicating that shocks are not a major excitation mechanism in EXor environments. Indeed, weak shock excited features below our sensitivity threshold have been detected in few cases (see Table 2): in particular we mention here the blue-shifted [FeII] emission lines (at  $1.53$  and  $1.64 \mu\text{m}$ ) likely associated with the spatially resolved jet of PV Cep (Hartmann et al. 1994).

By looking at the near IR continuum shape of our sources, a broad water absorption feature near  $1.9 \mu\text{m}$  seems recognizable in some objects (mainly XZ Tau, UZ Tau and VY Tau). Some evidence appears also in favour of a similar water feature near  $1.4 \mu\text{m}$ , which usually goes with the  $1.9 \mu\text{m}$  one in very late low mass stars and brown dwarfs (Lançon & Rocca-Volmerange 1992). These three sources indeed present the latest spectral types among the EXor sample and display also and other (NaI, CaI) photospheric absorptions (see Sections 4.3 and 4.4), suggesting a similar origin for the water bands, as well.

As a general trend, the observed spectra of the EXor are much more similar to those of accreting T Tauri stars (Greene & Lada 1996) than the FUor ones. All these latter have spectra always dominated by absorption lines (Reipurth & Aspin 1997), apart a couple of exceptions.

Spectroscopic variability is more or less evident in all the monitored sources and is often accompanied by significant variations of the line equivalent widths (see Tables from 3 to 9);

this means that spectroscopical variations are not a mere consequences of the continuum ones, but they are related to the source brightness through a less trivial link.

## 4. Discussion

Before analyzing in the next Sections the results of our near-IR spectral survey, we shortly comment on the variability presented by the EXor near-IR spectra collected so far in the literature.

The last 30 years of near-IR spectroscopic results of EXor are summarized in Table 10 along with the data of the present survey given in boldface). Literature data are available only for the indicated transitions and are given in form of calibrated flux densities or equivalent width (EW), accordingly to the original papers. This twofold way of presenting the data forces us to examine line flux and EW variability of a given source as two separate sets. A first glance at Table 10 indicates that only 14 spectra in total were known prior of our survey, hence it is clearly evident that studying IR line variability of EXor has not represented so far a major interest, despite of the significant spectral changes detected at optical wavelengths that, however, sample inner and warmer regions. The past few and sparse observations indicate that some IR line variation (by about a factor of 2) was recognizable but on very uncertain timescales. Taking into account also our data, we can estimate an IR line variability from a factor of 2 up to an order of magnitude and typical timescales from months to years, respectively.

### 4.1. Spectroscopic vs. photometric variability

The initial results of our ongoing survey are plotted in Figures 8 and 9, where the fluxes of few prominent lines observed in different dates are depicted as a function of the source brightness in the corresponding band (J for  $\text{Pa}\beta$  and  $\text{Pa}\gamma$  and K for  $\text{Br}\gamma$  and  $\text{CO (2-0)}$ ). We remind that spectroscopy and photometry are contemporary. Together with the new results, we include for completeness also our data of V1118 Ori as anticipated above. By examining both Figures, we see that the H recombination lines plots show a similar behaviour, while the  $\text{CO 2-0}$  correlation with the K mag appears quite different since this feature is detected both in emission (solid symbols) and in absorption (open symbols) for different continuum levels. The recombination lines exhibit an overall trend, according to which the brightest line fluxes are associated to brightest sources. Moreover, some sources (VY Tau, DR Tau, NY Ori and PV Cep) present line fluxes which tend to increase as the continuum increases. This

consideration seems not to be applicable to all the individual sources; indeed, XZ Tau and UZ Tau show constant line fluxes while the source brightens, although by a small amount (less than 0.5 mag). Two interesting cases are represented by V1118 Ori and PV Cep. Both sources exhibit a large continuum variation ( $\Delta J \gtrsim 1.2$  mag,  $\Delta K \gtrsim 1.0$  mag the former, and  $\Delta J \gtrsim 2.2$  mag,  $\Delta K \gtrsim 1.2$  mag the latter) associated with a significant (more than a factor of 6 and 2, respectively) flux variation of the recombination lines. Noticeably, V1118 Ori is the only source deliberately monitored for a longer time during a post-outburst phase, while monitoring the fading phase of PV Cep has been fortuitous, since this source belongs to the targets of our unbiased monitoring accomplished so far on a period of only one year, in principle too short to document significant variations. The sources for which the largest continuum variations (more than one mag) have been sampled, are those presenting a definite line flux increase as the continuum increases; conversely, objects showing smaller continuum fluctuations (less than half mag), show more erratic line variations and cannot be directly correlated to continuum variations, but are more likely related to local instabilities. Our preliminary conclusions need to be confirmed by continuing our IR monitoring in order to adequately sample larger variations (both in continua and lines) whose existence, according to literature data (Paper II), is well documented. The following preliminary analysis will be essentially based on a restricted sub-sample of sources that present at the moment a significant number of HI recombination lines, namely those for which a reasonable fitting can be applied (see next Sect. 4.2.1). This small sample is constituted by the spectra taken in different epochs of UZ Tau, DR Tau, V1118 Ori, and PV Cep.

Whatever is (are) the mechanism(s) responsible for line emission, it is worthwhile to investigate whether extinction has a role in determining the photometric and spectroscopic variability of EXor's. To that scope, the JHK photometry contemporary to the spectra (see Table 2) is provided in form of two colours diagram. The colour variations of the four sources of our sub-sample are depicted in Figure 10 and marked with progressive numbers pertaining to different epochs. For comparison purposes, in the same plot all the results of our photometric monitoring are displayed: the solid (open) symbols indicate that a contemporary near-IR spectrum exists (is absent). Figure 10 gives also the extinction vector (Rieke & Lebofsky 1985) starting from both the unreddened main sequence (solid line) and the locus of T Tauri stars (dashed line - Meyer et al. 1997).

The objects that during our monitoring period have shown the smallest fluctuations (ie. UZ Tau E and DR Tau) are, as expected, associated to negligible color variations, apparently not related to any extinction variation. Out the two sources showing the largest photometric variations (V1118 Ori and PV Cep), the former presents some indications in favour of an extinction dependance, but we think this occurrence may be fortuitous since our



prior photometric monitoring evidenced an erratic change of position on the same two colours plot (Fig.2 of Paper I). Moreover, if the extinction variation of V1118 Ori between the two epochs (ie.  $\Delta A_V \simeq 2.5$ ) were genuine, it should not be enough to account for the observed Br $\gamma$  fading by more than a factor of six. The colours of the remaining EXor monitored so far do not show any extinction dependance either.

The sole source for which a variable extinction seems to be the most plausible reason for its photometric and spectroscopic fluctuations is PV Cep. By comparing the photometric data (Table 2) and its consequent location in Figure 10 along the extinction vector, one can see that all the bright phases correspond to diminishing  $A_V$  values, while fading is always associated with an  $A_V$  increasing. More quantitatively,  $A_V$  has varied between 9.0 and 14.5 mag during our monitoring period (see also Table 11). We have corrected the observed line fluxes (just Pa $\beta$  and Br $\gamma$  for having a check) by using the adequate  $A_V$  as derived from the photometry of that epoch (Figure 10): by doing so, the intrinsic Pa $\beta$  and Br $\gamma$  fluxes relative to different dates become substantially equal (within a factor lesser than 1.5) and the intrinsic line ratios Pa $\beta$ /Br $\gamma$  remain all in the range 2.5-3.5 (Table 11). This result gives strong support to the hypothesis that line flux variation in PV Cep are due to a variable extinction more than to modification in the accretion (or mass loss) rate.

Such  $A_V$  variation can be translated into the volume density needed to pass from  $A_V = 9.0$  to  $A_V = 14.5$  through the relationship giving the column density,  $N(\text{H}_2) = A_V 10^{21}/R \text{ cm}^{-2}$ , where R represents the size of the obscuring matter. Even assuming a size equal to 5 stellar radii of a M0 star, we would obtain a volume density  $n \simeq 4 \cdot 10^9 \text{ cm}^{-3}$ , a value surprisingly high if it were uniformly distributed on such a large volume. Instead, a similar amount of dust can be supposed as organized in much smaller structures, such as disk inhomogeneities, that repeatedly cross the line of sight. Indeed, the time elapsed from maximum to minimum light (80 days) is largely enough to cover many tens of stellar radii by travelling at the Earth velocity.

The fact that PV Cep is a peculiar young object was already stated many years ago (Cohen et al. 1981), through studies of the varying bi-conical nebula associated to the star (GM29 - Gyl'budagyan & Magakyan 1977). This object shows simultaneously continuum variations due to extinction and episodic mass ejection phenomena. Indeed, the fan-shaped morphology of the varying nebula and the strongest P-Cygni profiles in the hydrogen lines at the maximum light suggest, respectively, that a circumstellar disk intermittently obscures the star and that the greatest brightness may occur close to the highest mass ejection events. Cohen et al. (1981) presented also optical continuum variations of PV Cep, whose time-scales and amplitudes are well in agreement with our observations. Further support to the disk presence is given by the ice absorption feature around 3  $\mu\text{m}$  that has been interpreted as a

common manifestation associated to edge-on morphologies (van Citters & Smith 1989).

The peculiarity of PV Cep (with respect to the other EXor’s) displayed by our data and confirmed by the literature, suggests some caveat in dealing with it as a confirmed member of the class. Maybe PV Cep could be an EXor in a less evolved stage as other candidates seem to be (see Sect. 4.5).

## 4.2. HI recombination

HI recombination lines largely dominate our near-IR spectra of EXor, hence we will rely on them to probe the gas emitting region and to discuss the correlation between line emission and continuum variability.

The debate whether near-IR hydrogen lines observed in T Tauri stars originate in the winds or arise in the accretion regions is still open: the former is supported by: (i) the univocal presence of winds; (ii) the presence of P-Cygni profiles; (iii) recent spectro-astrometric studies of T Tauri stars (Whelan, Ray & Davis 2004); (iv) the same magnetospheric accretion models. Analogously, also the mass accretion scenario (e.g. Hartmann, Hewett & Calvet 1994) sits on theoretical (e.g. Shu et al. 1994) and observational (e.g. Kenyon et al. 1994) basis. Winds and accretion flows may concur to originate the hydrogen line emission: both environments are opaque to the Lyman continuum photons, but hydrogen is photoionized, in any case, by the Balmer continuum photons (Natta et al. 1988; Basri & Bertout 1989). Whatever is the emission region (infall envelope or wind), it is worthwhile noting that the powering mechanism is likely the same, namely the accretion which onsets the wind.

In the framework of the wind hypothesis, we model the behaviour of those sources where a significant number of HI recombination lines have been observed with a wind model (Nisini, Antonucci & Giannini 2004) that considers a spherically symmetric envelope with a constant rate of mass loss ( $\dot{M} = 4\pi r^2 \rho(r) v(r)$ ). The emitting gas is assumed to be in LTE and the adopted gas velocity law is:

$$v(r) = v_i + (v_{max} - v_i)[1 - (R_*/R)^\alpha] \quad (1)$$

where  $v_i$  and  $v_{max}$  are the initial and maximum wind velocities, respectively, while  $R_*$  is the stellar radius. The best fit to the data points is obtained for the set of parameters, namely the envelope size  $R_{out}$  (expressed in units of stellar radii  $R_*$ ) and the gas temperature  $T$ , given in columns 4 and 5 of Table 11, respectively. We have assumed input values equal for

all the objects for the remaining parameters, they are: the initial gas velocity  $v_i = 30 \text{ km s}^{-1}$ ; the envelope's internal radius  $R_i = 1 R_*$ , where  $R_*$  has the value corresponding to the stellar spectral type; and the exponent  $\alpha = 0.2$ . The adopted  $A_V$  values (col.2 of Table 11) are taken from the literature (Table 1) or from our photometry. For the investigated sources, some model fitting to the data are depicted in Figures 11 to 13, as an example; observational data are shown as line ratios of the Paschen and Brackett series with respect to the  $\text{Pa}\beta$  and  $\text{Br}\gamma$ , respectively.

To evaluate the uncertainties on the derived parameters and to check the sensitivity of our model, we computed the range of variation for each input parameter that is allowed to eventually provide line flux predictions comparable (within a 50 % extent) to the observed values. Such analysis indicates that gas temperature is one of the less sensitive parameters: variations between 5000 K and 10000 K do not affect the fit significantly. Conversely, other parameters are quite critical and their variability ranges are consequently rather narrow: about 50 % for  $\dot{M}$ ,  $R_i = 1 - 2 R_*$ , 50 % for the envelope thickness. Table 11 gives, for each date, the ratio between the observed (corrected for extinction) and predicted (by our model) values of  $\text{Pa}\beta$  (col.6) and  $\text{Br}\gamma$  (col.7).  $\text{Pa}\beta/\text{Br}\gamma$  ratios, both predicted (col.8) and observed (col.9) are listed, as well. Such a comparison (observations vs. model) allows us to verify the goodness of the obtained fit. Due to the uncertainties of the observations and even more to those of modelling, we assume that fit to the data can be considered as acceptable when (i) the ratios  $\text{Pa}\beta(\text{mod}/\text{obs})$  and  $\text{Br}\gamma(\text{mod}/\text{obs})$  range between 0.7 and 1.5; and (ii) the ratio  $\text{Pa}\beta/\text{Br}\gamma$  derived from the model does not differ from the observed one by more than 50%. Such requirements are well fulfilled in all cases listed in Table 11. The sole exception is represented by some values of PV Cep (see the caveat in Sect.4.1), which indeed shows observed ratios  $\text{Pa}\beta/\text{Br}\gamma$  lower than those of other sources and not compatible with any reasonable combination of input parameters. Finally column 10 of Table 11 lists the mass loss rate ( $\dot{M}_{\text{wind}}$ ) derived from our model: these values range between  $10^{-8}$  and  $10^{-7} M_\odot \text{ yr}^{-1}$  (apart two determinations for PV Cep), namely they are consistent with the range of values inferred by independent determinations on active T Tauri stars (Hartigan, Edwards & Ghandour 1995).

$\text{Pa}\beta$  and  $\text{Br}\gamma$  line luminosity can be also independently used to get an estimate of the  $\dot{M}_{\text{acc}}$  to be compared with  $\dot{M}_{\text{wind}}$  derived by our model. To that scope, the empirical relationships given by Muzerolle, Hartmann & Calvet (1998) can be used. It relates the emission line ( $\text{Pa}\beta$  and  $\text{Br}\gamma$ ) luminosities with the accretion luminosity as measured from the continuum excess. We remark how the empirical nature of such relationships allows us their applications whatever is the origin of the recombination lines (accretion or wind). Table 12, for each date, provides: the positive or negative luminosity variation (integrated just over the JHK bands - col.3) with respect to luminosity value obtained in the first epoch; the

extinction correction applied for deriving the intrinsic fluxes (col.4); the accretion luminosities values derived from the equations (1) and (2) of Muzerolle et al. (1998) (col.5 and 6); From the accretion luminosity an estimate of the mass accretion rate can be derived (col.7) (Gullbring et al. 1998) by assuming the inner radius of the accretion disk  $R_i$  ( $R_i = 5 R_*$ ), the stellar mass ( $M_*$ ), and the stellar radius ( $R_*$ ) according to the spectral type indicated for each source in Table 1. The derived mass accretion rates roughly exceed by an order of magnitude the mass loss ones, as predicted by wind models (see Sect.1).

Therefore we can conclude that the wind scenario alone is fully consistent with the observational data. However, we are not able to rule out that the same HI lines can be originated by accretion alone. Indeed, this latter can account for the observed  $\text{Pa}\beta/\text{Br}\gamma$  ratios (roughly between 3 and 4, see Table 11) only for  $\dot{M}_{acc} > 10^{-8} M_\odot \text{ yr}^{-1}$  (Muzerolle, Calvet & Hartmann 2001 - their Figure 15). Unfortunately, accretion models able to quantitatively predict in a consistent way also wind emission do not exist, hence, within this scheme, it is not easy to verify any consistence between  $\dot{M}_{wind}$  and  $\dot{M}_{acc}$ .

### 4.3. CO overtone emission

CO emission is seen together with  $\text{Br}\gamma$  line emission, but these two features probably come from different volumes of gas. At temperatures of about 4000 K, both CO and molecular hydrogen are dissociated by collisions. However, for density values higher than  $10^7 \text{ cm}^{-3}$  and in the presence of  $\text{H}_2$ , CO dominates the cooling (Scoville et al. 1980). Therefore CO bands are specific probes of the circumstellar portions where the gas is relatively warm at high densities. Recently interferometric observations of CO emission in PMS objects have confirmed that CO comes from a small region ( $< 1 \text{ AU}$ ), i.e. the inner gaseous disk (Tatulli et al. 2008), much more compact than that typical of the  $\text{Br}\gamma$  emission, i.e. the stellar wind (Malbet et al. 2007). However, young stars emitting  $\text{Br}\gamma$  from regions more compact than the dust sublimation radius, have been found, as well (Kraus et al. 2008).

A number of models have been proposed for producing CO emission (for a summary see: Biscaya et al. 1997). Carr (1989) investigated an accretion disk and a neutral stellar wind scenario. Inner circumstellar disk regions (Najita et al. 1996), or infalling material heated by adiabatic compression from 3000 to 6000 K (Martin 1997), have been also proposed as regions where CO emission may arise.

However, as anticipated in Sect.3, CO overtone features [typically (2-0) and (3-1)] behave in a quite variable manner in EXor. With reference to Figure 9 (bottom panel) the spectra of

some sources (DR Tau, V1118 Ori and NY Ori) present CO bands in emission (solid symbols) or in absorption (open symbols) on different epochs. For the remaining sources, CO bands, although largely variable, have been detected always in emission or always in absorption, during our monitoring period. Trying to understand whether CO features are related to the continuum emission, we concentrate our attention on the couple of sources (V1118 Ori and PV Cep) that exhibit the largest (i.e the most significant) continuum variations ( $\Delta K > 1$  mag). While brightening, V1118 Ori presents CO features passing from absorption to emission and PV Cep presents emission features of increasing intensity. This trend is the same described above (see Sect.1) for V1647 Ori, the eruptive variable recently discovered.

A plausible interpretation of our observations can be given in terms of two prevailing mechanisms. If we assume that CO absorption is originated in the stellar photosphere (ref.), then it can be detected only during the more quiescent phases when the accretion rate is low, the continuum emission is low as well, and the star surface is more easily visible. When the accretion rate increases, it produces a significant increase of the UV radiation at the accretion shock that in turn heats the inner disk favoring CO emission associated to an enhanced continuum emission. It is worthwhile to continue our spectroscopical monitoring to confirm or not the proposed scenario. A further evidence that stellar surface is more easily visible at minimum brightness was already presented in Fig.6 of Paper II where we noticed how, near the minimum, higher and more variable values of polarization were detected, suggesting that, in such conditions, we can see the heavy spotted and magnetized photosphere.

#### 4.4. NaI feature at 2.206 $\mu\text{m}$

Given its low first ionization potential (5.1 eV), sodium can be present close to low mass late type stars (like EXor, T Tauri) and in regions capable to shield direct ionizing photons from earlier type stars (e.g. circumstellar disks). The ionization structure of the emitting region can be suitably traced by the flux ratio  $\text{Br}\gamma/\text{NaI}$ , which is free by extinction effects because of the closeness in wavelength between the two permitted lines. Hydrogen is expected to be neutral in  $\text{Na}^+$  region, thus a low value of the  $\text{Br}\gamma/\text{NaI}$  ratio suggests a lower ionization; it might indicate the presence of high density regions where photons cannot easily penetrate.

In the presented EXor spectra the NaI 2.206  $\mu\text{m}$  unresolved doublet is detected both in emission and in absorption and, remarkably, this line follows the same behaviour than that of the CO bands. This circumstance is depicted in Figure 14, where the ratio CO 2-0/NaI is plotted vs the  $\text{Br}\gamma/\text{NaI}$  ratio for the different spectra taken in different monitoring phases.

Because of the closeness of the three transitions ( $2.166$ ,  $2.206$  and  $2.293 \mu\text{m}$   $\text{Br}\gamma$ ,  $\text{NaI}$  and  $\text{CO } 2\text{-}0$ , respectively), also this plot is unaffected by extinction. The  $\text{CO } 2\text{-}0/\text{NaI}$  values are all positive (two spectra of DR Tau represent the only exception), this means that  $\text{NaI}$  and  $\text{CO}$  are seen either both in emission or both in absorption. Since  $\text{Br}\gamma$  is detected always in emission, the  $\text{NaI}$  emission cases are located in the first quadrant (upper right) while  $\text{NaI}$  absorption are those in the second quadrant (upper left). Such a behaviour speaks in favour of a common origin for both  $\text{NaI}$  and  $\text{CO}$  features. Hence, following the interpretation given for  $\text{CO}$  features (Sect. 4.2),  $\text{NaI}$  line as well can be originated at the star photosphere (absorption) or in the inner disk (emission), depending on the outbursting stage of the object. Confirmation that  $\text{CO } (2\text{-}0)$  and likely fluorescent  $\text{NaI}$  emission at  $2.206 \mu\text{m}$  can arise in the same low excitation region is provided by McGregor et al. (1988), who note that carbon monoxide and sodium require similar temperatures to survive: the former is collisionally excited and emits at  $3000\text{-}4000 \text{ K}$ , as discussed in Sect.4.2; the latter is shielded in the same high density environment and is excited by adequate pumping photons without radiatively ionizing  $\text{NaI}$ .

Figure 14 shows how the values of the ratio  $F(\text{CO } 2\text{-}0)/F(\text{NaI})$  corresponding to emission cases are systematically larger (they cluster in the range 2-4) than those of absorption cases (between 1 and 2). This trend is likely related to the different physical conditions between the stellar photosphere and the circumstellar environment.

Antoniucci et al. (2007) noticed that the ratio  $\text{Br}\gamma/\text{NaI}$  for jet driving sources ranges between 2 and 5, while larger values are associated to Class I sources that show no evidence of jet emission. The ratios we have obtained for the EXor (see Figure 14) are low and in the same range of the former group, although the presence of a jet does not seem a property applicable to the EXor class. A plausible explanation is that the low value of ratio  $\text{Br}\gamma/\text{NaI}$  is typical of those cases where the role of the circumstellar disc dominates.  $\text{NaI}$  IR emission lines, be they associated to jet driving sources or to EXor variables, come from large columns of warm and neutral material located in the inner part of the disc.

Finally, we note that all the objects that present  $\text{NaI}$  in absorption have also  $\text{CaI}$  in absorption at  $2.267 \mu\text{m}$ , at a comparable intensity level. This provides further support to the hypothesis that the stellar photosphere appears during the most inactive phases.

#### 4.5. Comparison with spectra of sources candidate to be EXor

In the recent years seven additional outbursting sources have been tentatively recognized as EXor, although the attribution to this class (or to the FUor one) is still debated. They

are listed in Table 13 along with some relevant parameters. The available near-IR spectra, apart one featureless exception, are all emission line spectra strictly resembling those of the EXors presented in Sect.3: in fact they are largely dominated by hydrogen recombination along with other ionic contributions and CO bandhead emission around  $2.3 \mu\text{m}$ . Moving from active to inactive phases line emission tends to fade and the  $P_{Cyg}$  profiles progressively diminish. Other feature in common with the classical EXor is the photometric behaviour generally becoming bluer while brightening (Paper II). All in all candidates and confirmed members appear quite equivalent with respect to their spectroscopic properties; a substantial difference is that the candidates are more embedded ( $A_V \gtrsim 10$  mag) than the other EXor, suggesting, not surprisingly, that this evolutionary stage might also occur earlier than the T Tauri phase.

## 5. Concluding Remarks

We have presented the first results of a long term spectroscopic monitoring of EXor in the near-IR aimed to investigate the variability in the accretion process, hence modalities and timescales of the process itself. By analyzing the results, the following can be summarized:

- The presented part of our database refers just to the starting period (2007-2008): more than 25 spectra have been obtained in different epochs and they correspond to 8 sources in total. To correlate continuum and line variability, all the observations are taken by performing simultaneous photometry (JHK bands) and low resolution ( $\mathcal{R} \sim 250$ ) spectroscopy in the near-IR ( $0.8$  to  $2.5 \mu\text{m}$ ).
- EXors near-IR spectra are line emission spectra dominated by hydrogen recombination (Paschen and Brackett series) signalling the presence of an ionized region. CO overtone features  $v=2-0$ ,  $v=3-1$  are commonly detected both in emission and in absorption and weaker atomic features (NaI and CaI) appear in emission or absorption following the CO behaviour. At our level of sensitivity, molecular hydrogen contributions are absent, suggesting that shocks do not represent a major mechanism of excitation. All in all EXor IR spectra look like those of the accreting T Tauri stars more than those of FUor objects.
- Dealing with the first results of a long term monitoring program, an attempt has been done to complement our data with literature spectra so far collected. The last 30 years of near-IR spectroscopic results of EXor, prior to our survey, consist in just 14 spectra. These very few and sparse observations only suggest that some line emission variability exists on very uncertain timescales. Complementing these data with the results of our

survey, we can estimate an IR line variability from a factor of 2 up to an order of magnitude and typical timescales from months to years, respectively.

- The sources for which the largest continuum variations (more than one mag) have been sampled, are those presenting a well defined HI line flux increase as the continuum increases; conversely, objects showing smaller continuum fluctuations (less than half mag), show more erratic line variations and cannot be straightforwardly associated to well characterized accretion events, but are more likely related to local instabilities.
- The possibility that line variability is due to a variable extinction has been explored, and appears well applicable only to the spectra taken in different epochs of the peculiar source PV Cep.
- The obtained spectra have been compared with a wind model that considers a spherically symmetric and partially ionized envelope with a constant rate of mass loss. Mass loss rates in the range  $2\text{--}10 \cdot 10^{-8} \text{ M}_{\odot} \text{ yr}^{-1}$  are derived along with additional wind parameters. A possible origin of HI lines from accretion is investigated and it also provides consistent results.
- CO overtone features have been detected both in emission and in absorption. They are highly variable even on a short (days to months) timescale. In particular, while brightening, one source presents CO features passing from absorption to emission and another presents emission features of increasing intensity. CO absorption could be originated in the stellar photosphere, thus it can prevail only during quiescent phases when the star surface is more easily visible. When the accretion rate increases the UV radiation at the accretion shock heats the inner disk favoring CO emission.
- NaI  $2.206 \mu\text{m}$  (and more rarely CaI  $2.267 \mu\text{m}$ ) is detected both in emission and in absorption and, remarkably, it follows what CO bands do. Consequently all these lines are thought to arise in the same regions: the photosphere (when in absorption), or the inner disk (when in emission).
- Finally, a comparison is made with the outbursting sources tentatively recognized as candidate EXor. They appear quite equivalent with respect to their spectroscopic properties; a substantial difference is that the candidates are more embedded than the other EXor, suggesting that this evolutionary stage might also occur earlier than the T Tauri phase.

A systematic investigation of the quantitative (inter-)relationship between line and continuum flux variations will be possible once our survey will achieve a longer coverage and hence a larger number of significant accretion events could be sampled.



## REFERENCES

- Acosta-Pulido, J.A., Kun, M., Ábrahám, P. et al. 2007, AJ,133, 2020
- Antoniucci, S., Nisini, B., Giannini, T. & Lorenzetti, D. 2007 A&A 479, 503
- Aspin, C., Beck, T.L., & Reipurth, B. 2008 AJ 135, 423
- Beck, T., McGregor, P.J., Takami, M. & Tae-Soo Pyo 2008 ApJ 676, 472
- Basri, G. & Bertout, C. 1989 ApJ 341, 340
- Beristain, G., Edwards, S. & Kwan, J. 1998 ApJ 499, 828
- Biscaya, A.M., Rieke, G.H., Narayanan, Gopal, Luhman, K.L. & Young E.T. 1997 ApJ 491, 359
- Bonnell, L. & Bastien, P. 1992 ApJ 401, L31
- Breger, M., Gehrz, R.D. & Hackwell, J.A. 1981 ApJ 248, 963
- Carr, J.S. 1989 ApJ 345, 522
- Carr, J.S. 1990 AJ 100, 1244
- Clarke, C., Lin, D. & Pringle, J. 1990 MNRAS 242, 439
- Coffey, D., Downes, T.P. & Ray, T.P. 2004 A&A 419, 593
- Cohen, M., Kuhl, L.V. 1979 ApJS, 41, 743
- Cohen, M., Kuhl, L.V., Harlan, E.A. & Spinrad, H. 1981 ApJ 245, 920
- Davis, C.J., Nisini, B., Takami, M. et al. 2006 ApJ 639, 969
- Davis, C.J., Stern, L., Ray, T.P. & Chrysostomou, A. 2002 A&A 382, 1021
- Doppmann, G.W., Greene, T.P., Covey, K.R. & Lada, C.J. 2005 AJ 130, 1145
- Elias, J.H. 1978 ApJ 224, 857
- Edwards, S., Fisher, W., Hillenbrand, L. & Kwan, J. 2006 ApJ 646, 319
- Edwards, S., Fisher, W., Kwan, J., Hillenbrand, L. & Dupree, A.K. 2003 ApJ 599, L41
- Eislöffel, J., Günter, E., Hessman, F.V. et al. 1991 ApJL 383, L19

- Evans II, N.J., Levreault, R.M., Beckwith, S. & Strutskie, M. 1987 ApJ 320, 364
- Folha, D.F.M. & Emerson, J.P. 1999 A&A 352, 517
- Folha, D.F.M. & Emerson, J.P. 2001 A&A 365, 90
- Gasparian, L.G., Melkonian, A.S., Ohanian, G.B. & Parsamian, E.S. 1990 *Flare Stars in Star Clusters, Associations, and the Solar Vicinity* Proc. 137th Symposium of the International Astronomical Union, Byurakan [Armenia], U.S.S.R., October 23-27, 1989. Editors, L.V. Mirzoyan, B.R. Pettersen, & M.K. Tsvetkov; Publ. Kluwer Academic, Dordrecht, The Netherlands, Boston, MA.
- Gibb, E.L., Rettig, T.W., Brittain, S.D. et al. 2006 ApJ 641, 383
- Giovanardi, C., Gennari, S., Natta, A. & Stanga, R. 1991 ApJ 367, 173
- Gómez, M. & Mardones, D. 2003 AJ 125, 2134
- Greene, T.P. & Lada, C.J. 1996 AJ 112, 2184
- Gullbring, E., Hartmann, L., Bricčeno, C. & Calvet, N. 1998 ApJ 492, 323
- Gyul’budagyan, A.L. & Magakyan, T. Yu. 1977 Pis’ma Astron. Zh. 3, 162
- Hamann, F., Simon, M., Carr, J.S. & Prato, L. 1994 ApJ 436, 292
- Hartigan, P., Edwards, S., & Ghandour, L. 1995 ApJ 452, 736
- Hartmann, L., Hewett, R. & Calvet, N. 1994 ApJ 426, 669
- Hartmann, L., Hinkle, K. & Calvet, N. 2004 ApJ 609, 906
- Hartmann, L. & Kenyon, S. 1985 ApJ 299, 462
- Herbig, G.H. 1989 Proc. of the ESO Workshop on *Low Mass Star Formation and Pre-Main Sequence Objects*, ed. B. Reipurth, p.233
- Herbig, G.H. 1990 ApJ 360, 639
- Herbig, G.H. 2007 AJ 133, 2679
- Herbig, G.H. 2008 AJ 135, 637
- Herbig, G.H. & Bell, K.R. 1988 Lick Obs. Bulletin No.1111
- Herbig, G.H., Aspin, C., Gilmore, A.C. et al. 2001 PASP 113, 1547

- Hodapp, K.W. 1999 AJ, 118, 1338
- Hodapp, K.W., Hora, J.L., Rayner, J.T. et al. 1996 ApJ 468, 861
- Jensen, E.L.N., Dhital, S., Stassun, K.G. et al. 2007 AJ 134, 241
- Kenyon, S.J., Hartmann, L., Hewett, R. et al. 1994 AJ 107, 2153
- Köhler, R., Petr-Gotzens, M.G., McCaughrean, M.J. et al. 2006 A&A 458, 461
- Königl, A. & Pudritz, R.E. 2000 Protostars and Planets IV - University of Arizona Press;  
eds V.Mannings, A.P.Boss, S.S Russell, p.759
- Kóspál, Á., Ábrahám, P., Acosta-Pulido, J. et al. 2007 A&A, 470, 211
- Kraus, S., Hofmann, K.-H., Benisty, M. et al. 2008 A&A, in press (arXiv:0807.1119)
- Lançon, A., & Rocca-Volmerange, B. 1992 A&A Supp. Ser. 96, 593
- Liseau, R., Lorenzetti, D. & Molinari, S. 1992 A&A 253, 119
- Lorenzetti, D., Giannini, T., Calzoletti, L. et al. 2006 A&A 453, 579 (Paper I)
- Lorenzetti, D., Giannini, T., Larionov, V.M. et al. 2007 ApJ 665, 1182 (Paper II)
- Malbet, F., Benisty, M., de Wit, W.-J. et al. 2007 A&A 464, 43
- Martin, S.C. 1997 ApJ 478, L33
- McGregor, P.J., Hyland, A.R. & Hillier, D.J. 1988 ApJ 324, 1071
- Menten, K.M., Reid, M.J., T., Forbrich, J. & Brunthaler, A. 2007 A&A 474, 515
- Meyer, M.R., Calvet, N. & Hillenbrand, L.A. 1997 AJ 114, 288
- Muzerolle, J., Calvet, N. & Hartmann, L. 2001 ApJ 550, 944
- Muzerolle, J., Hartmann, L. & Calvet, N. 1998 AJ 116, 2965
- Najita, J., Carr, J.S., Glassgold, A.E., Shu, F.H. & Tokunaga, A.T. 1996 ApJ 462, 919
- Nisini, B., Antonucci, S. & Giannini, T. 2004 A&A 421, 187
- Reipurth, B. & Aspin, C. 2004 ApJ 606, L119
- Reipurth, B., Guimarães, M.M., Connelly, M.S. & Bally, J. 2007, AJ 134, 2272

- Sato, S., Nagata, T., Tanaka, M. & Yamamoto, T. 1990 ApJ 359, 192
- Rieke, G.H. & Lebofsky, M.J. 1985 ApJ 288, 618
- Scoville, N.Z., Krotkov, R. & Wang, D. 1980 ApJ 240, 929
- Sicilia-Aguilar, A., Merín, B., T., Hormuth, F. & Ábrahám, P. 2008 ApJ 673, 382
- Shu, F.H., Najita, J.R., Ostriker, E. et al. 1994 ApJ 429, 781
- Shu, F.H., Najita, J.R., Shang, -H. & Li, Z.-Y. 2000 Protostars and Planets IV - University of Arizona Press; eds V.Mannings, A.P.Boss, S.S Russell, p.789
- Stecklum, B., Melnikov, S.Y., & Meusinger, H. 2007 A&A 463, 621
- Takami, M., Chrysostomou, A., Ray, T.P. et al. 2006 ApJ 641, 357
- Tatulli, E., Malbet, F., Menard, F. et al. 2008 A&A, in press (arXiv:0806.4937)
- Vacca, W.D., Cushing, M.C. & Simon, T. 2004 ApJ 609, L29
- van Citters, G.W. & Smith, R.G. 1989 AJ 98, 1328
- Walter, F.M., Stringfellow, G.S., Sherry, W.H., & Field-Pollatou, A. 2004 ApJ 128, 1872
- Whelan, E.T., Ray, T.P. & Davis, C.J. 2004 A&A 417, 247

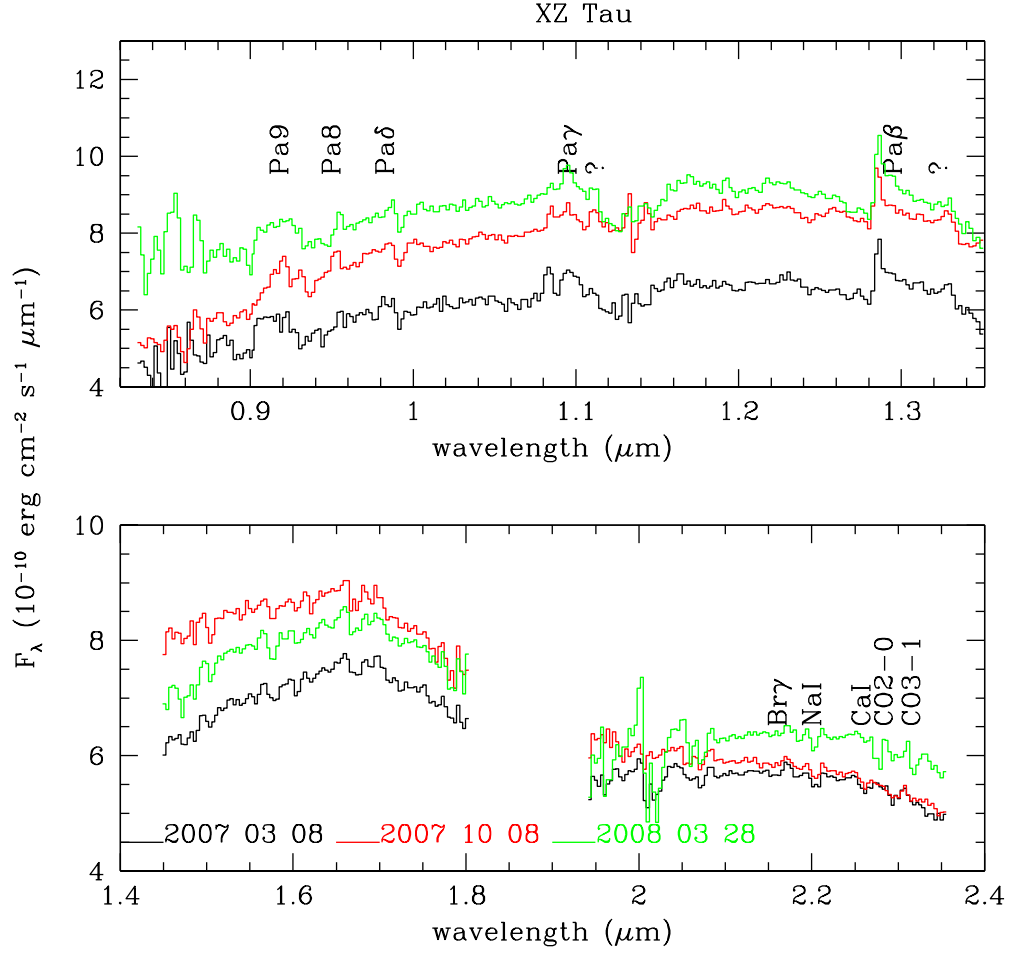


Fig. 1.— Near IR spectrum of XZ Tau. Detected line are identified and listed in Table 3.

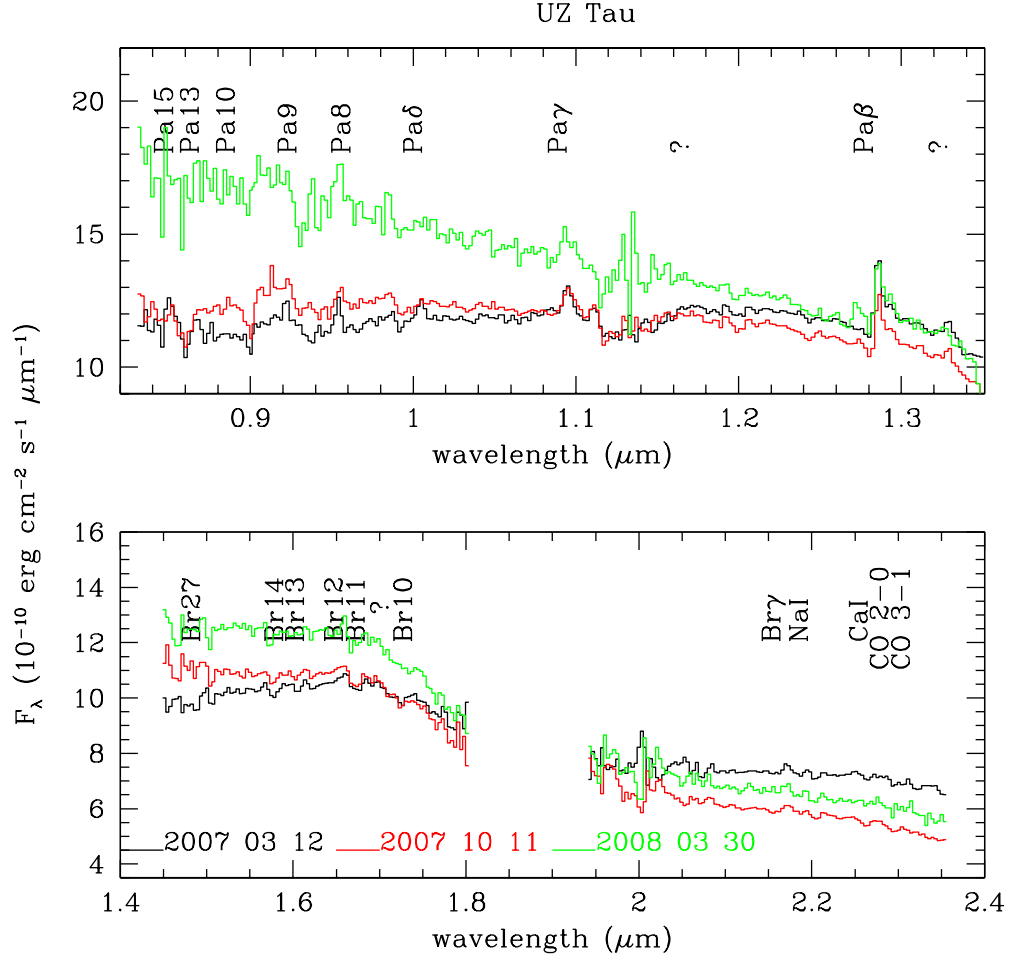


Fig. 2.— Near IR spectrum of UZ Tau. Detected line are identified and listed in Table 4. E and W components are not resolved in the spectral mode.

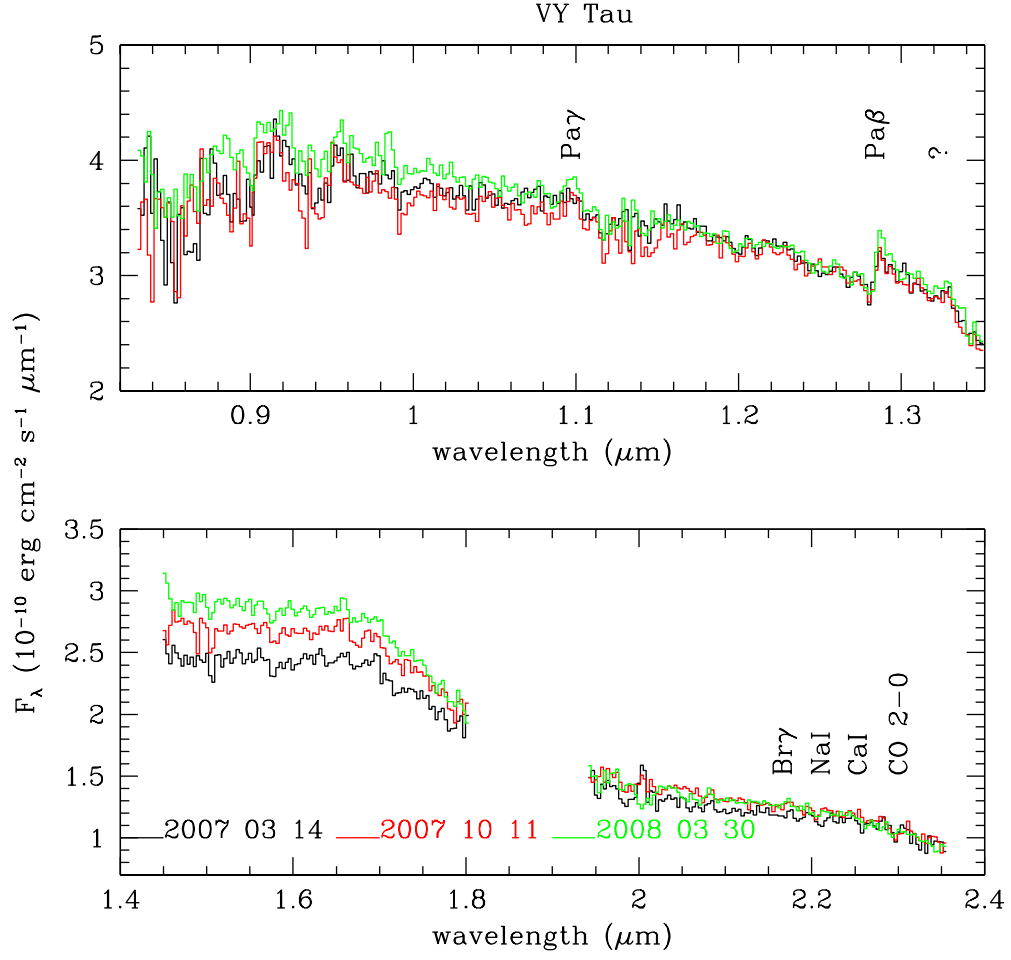


Fig. 3.— Near IR spectrum of VY Tau. Detected line are identified and listed in Table 5.

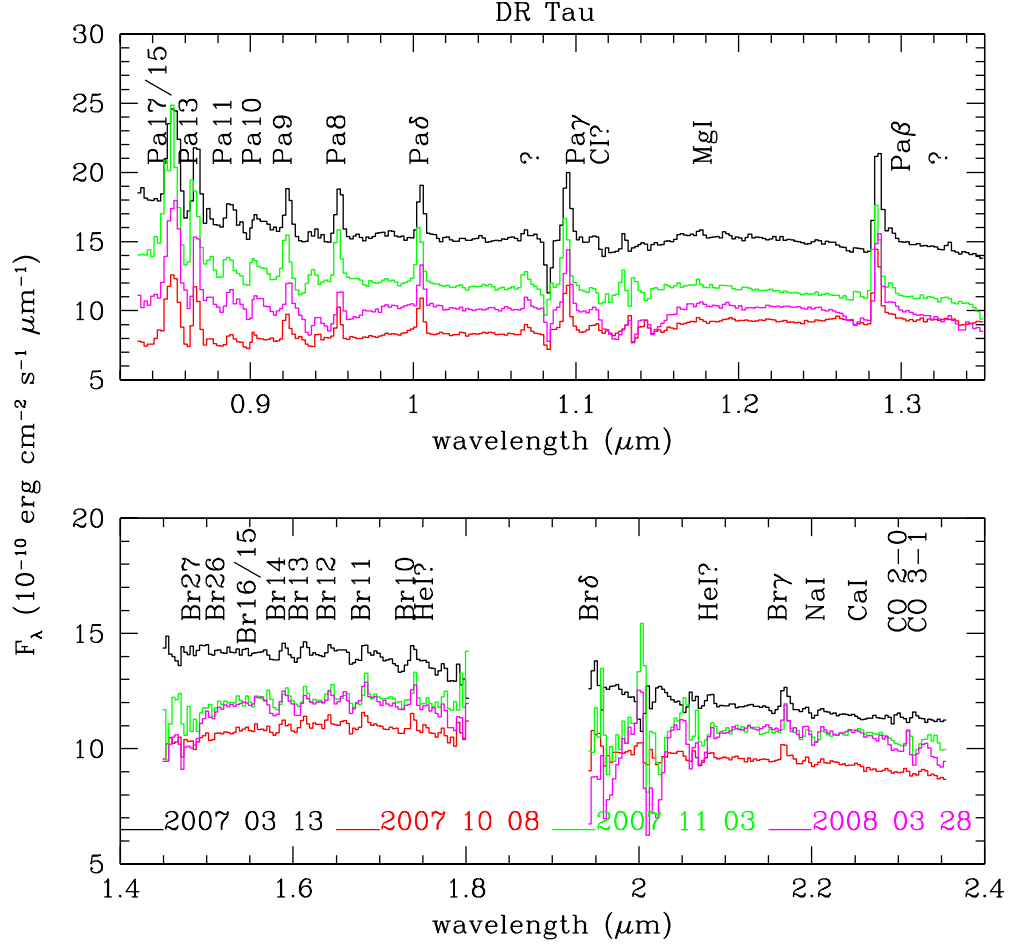


Fig. 4.— Near IR spectrum of DR Tau. Detected line are identified and listed in Table 6.



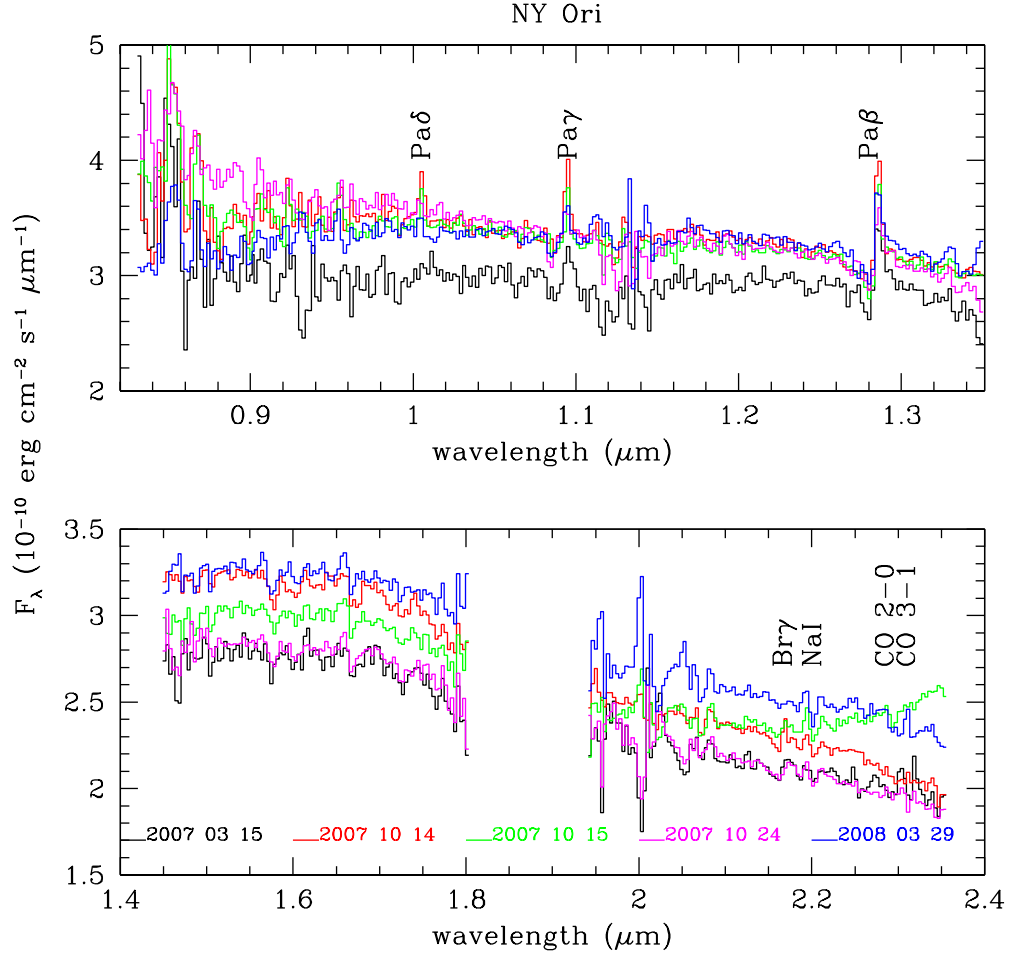


Fig. 5.— Near IR spectrum of NY Ori. Detected line are identified and listed in Table 7.

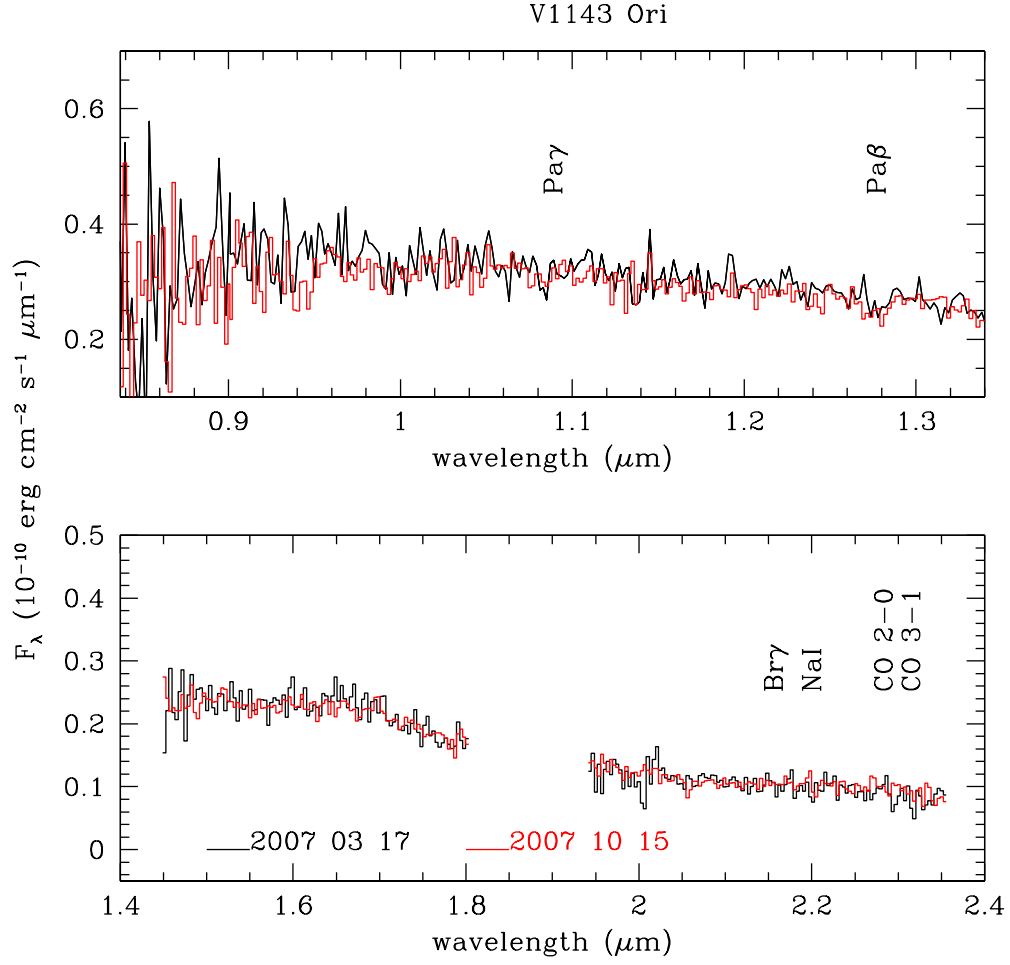


Fig. 6.— Near IR spectrum of V1143 Ori. Detected line are identified and listed in Table 8.

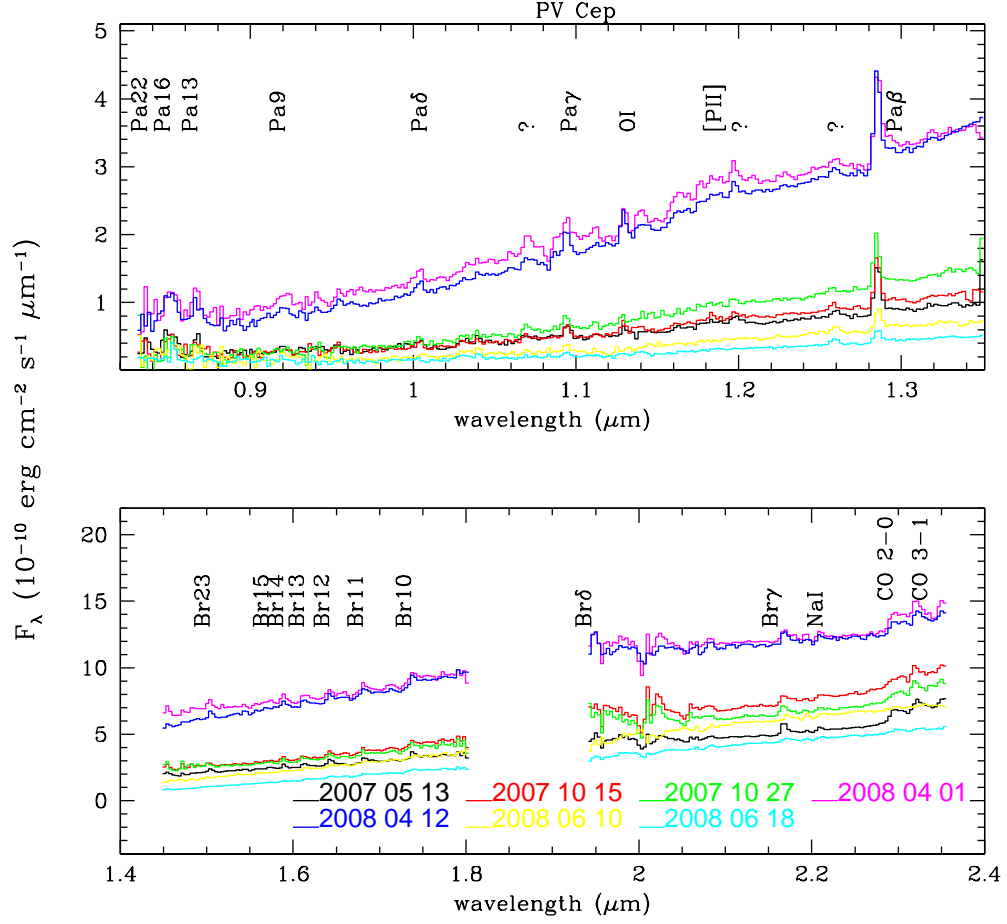


Fig. 7.— Near IR spectrum of PV Cep. Detected line are identified and listed in Table 9.

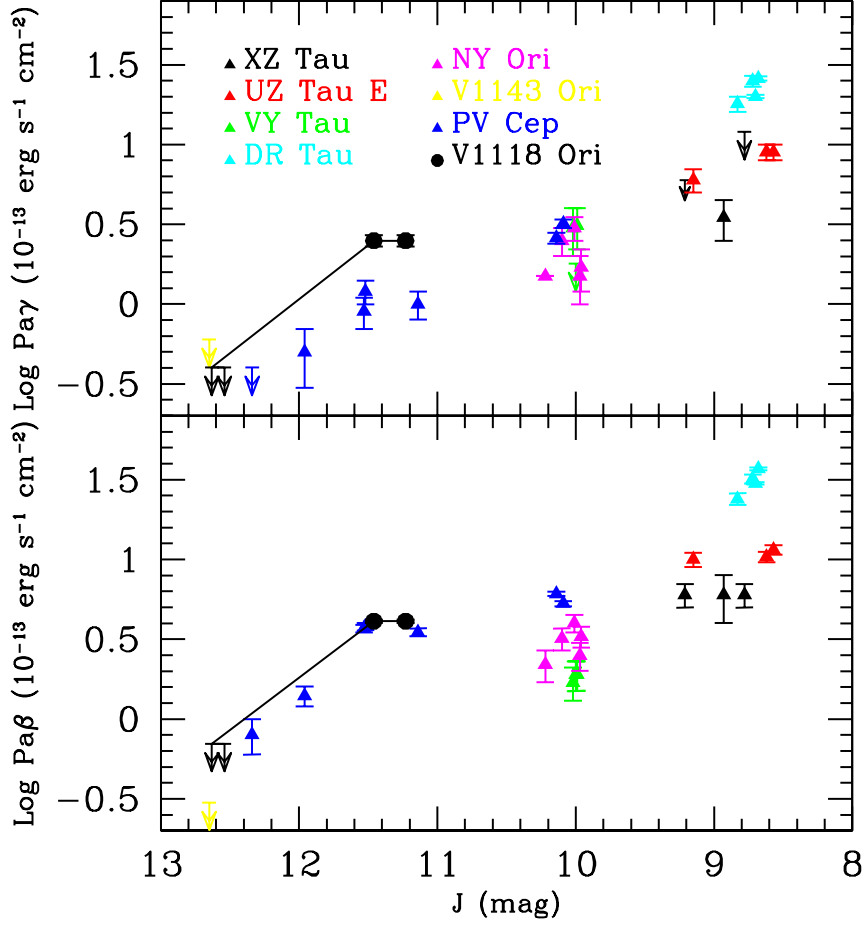


Fig. 8.— Observed Pa $\gamma$  and P $\beta$  fluxes as a function of brightness in the J band. Data points of the source V1118 Ori are connected with a straight line.

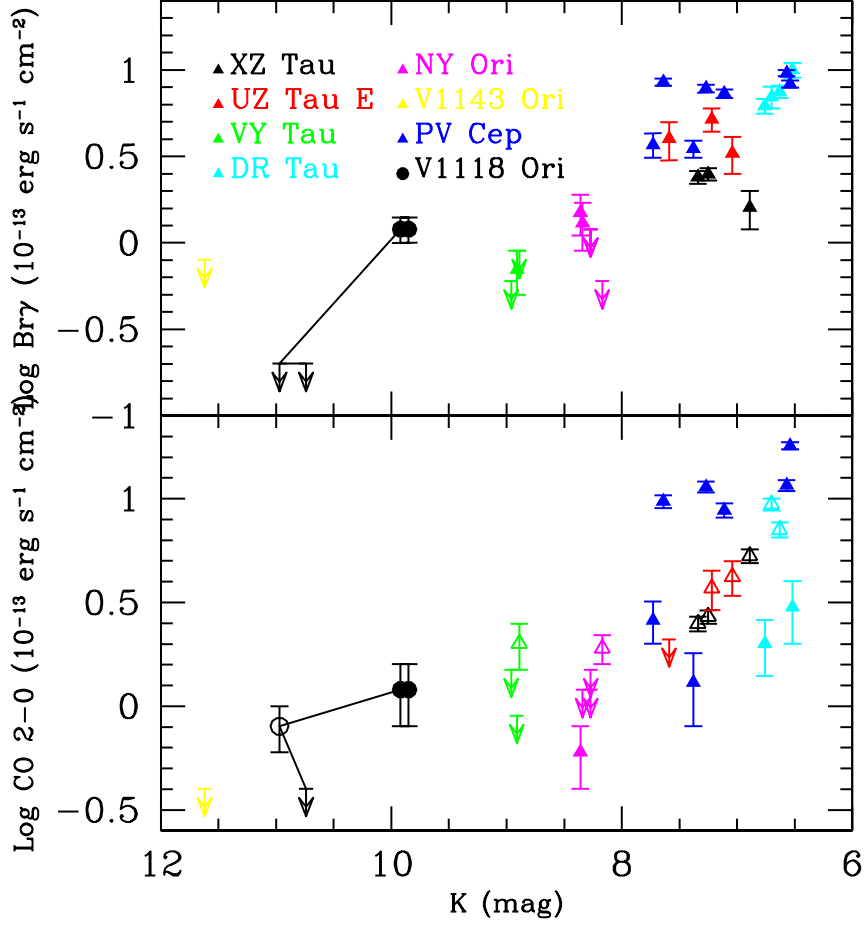


Fig. 9.— Observed Br $\gamma$  and CO 2-0 fluxes as a function of brightness in the K band. Open symbols indicate that CO line is in absorption. Data points of the source V1118 Ori are connected with a straight line.

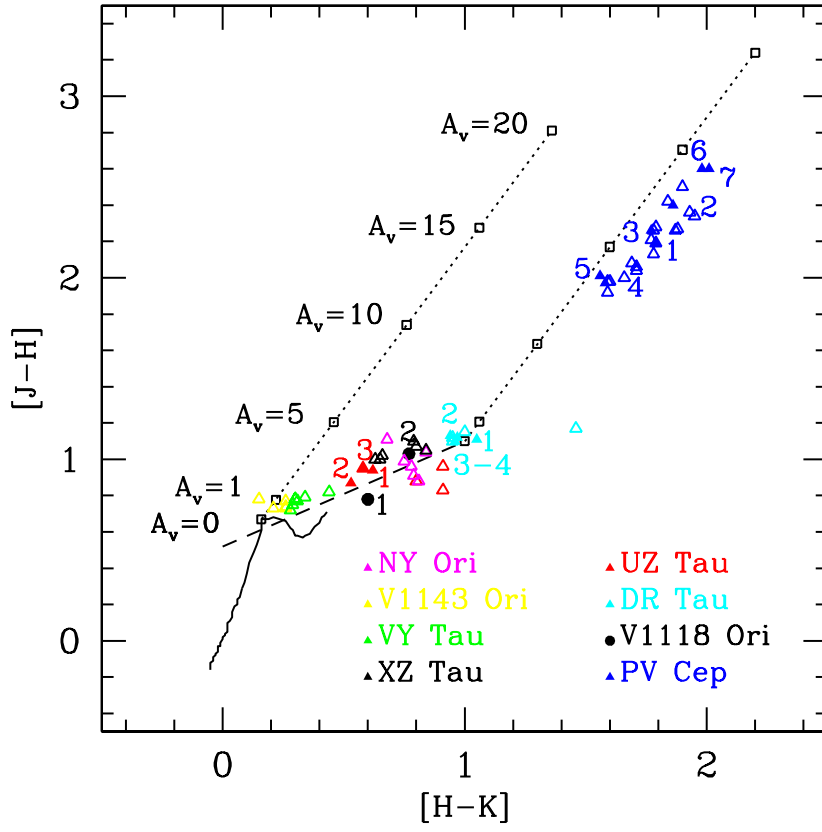


Fig. 10.— Near-IR two colours diagram of a selected sub-sample of EXor (see text) in different epochs. The solid line marks the unreddened main sequence, whereas the dashed one is the locus of the T Tauri stars (Meyer et al. 1997). Dotted lines represent the reddening law (Rieke & Lebofsky 1985) where different intervals of  $A_V$  (in mag) are indicated by open squares.

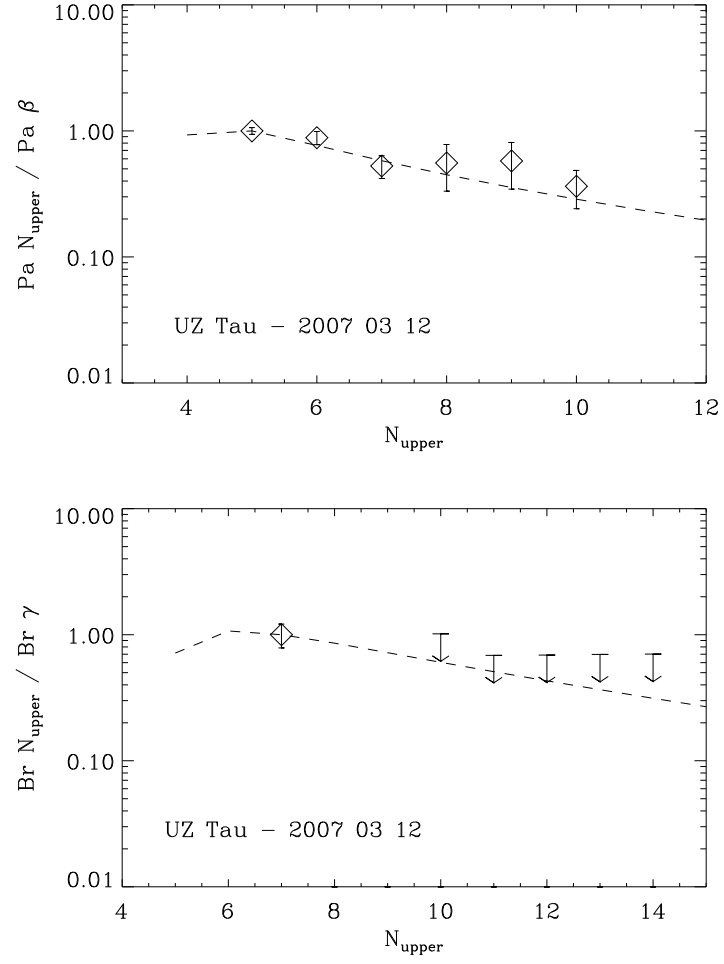


Fig. 11.— Line ratios of the Paschen (top) and Brackett (bottom) series for UZ Tau obtained in the indicated date. The best fit (dashed line) parameters are given in Table 11.

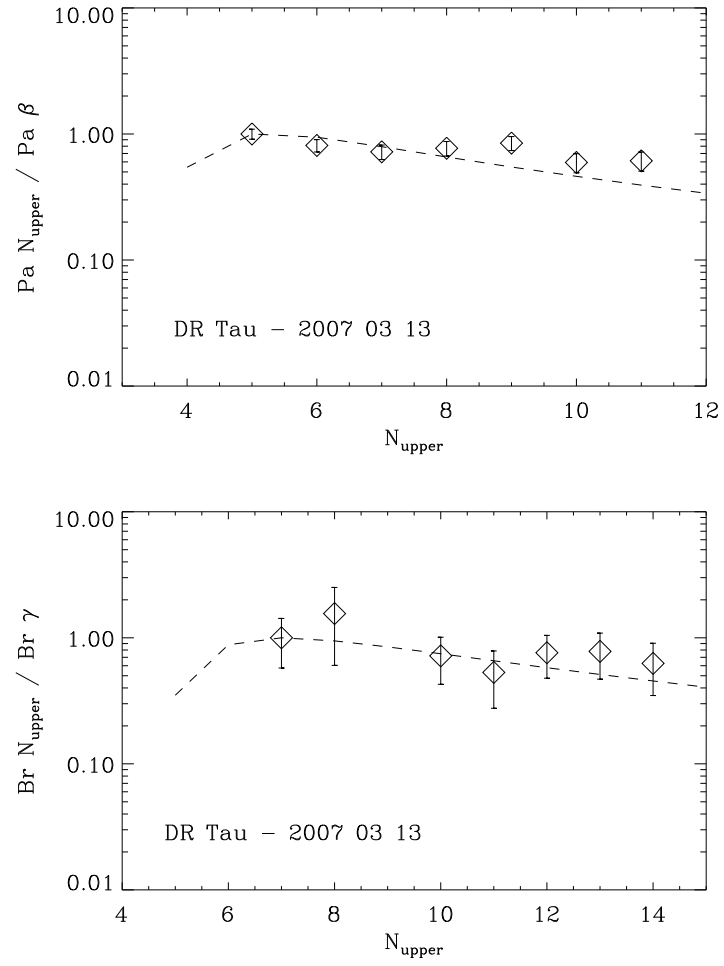


Fig. 12.— As Figure 11 for DR Tau.



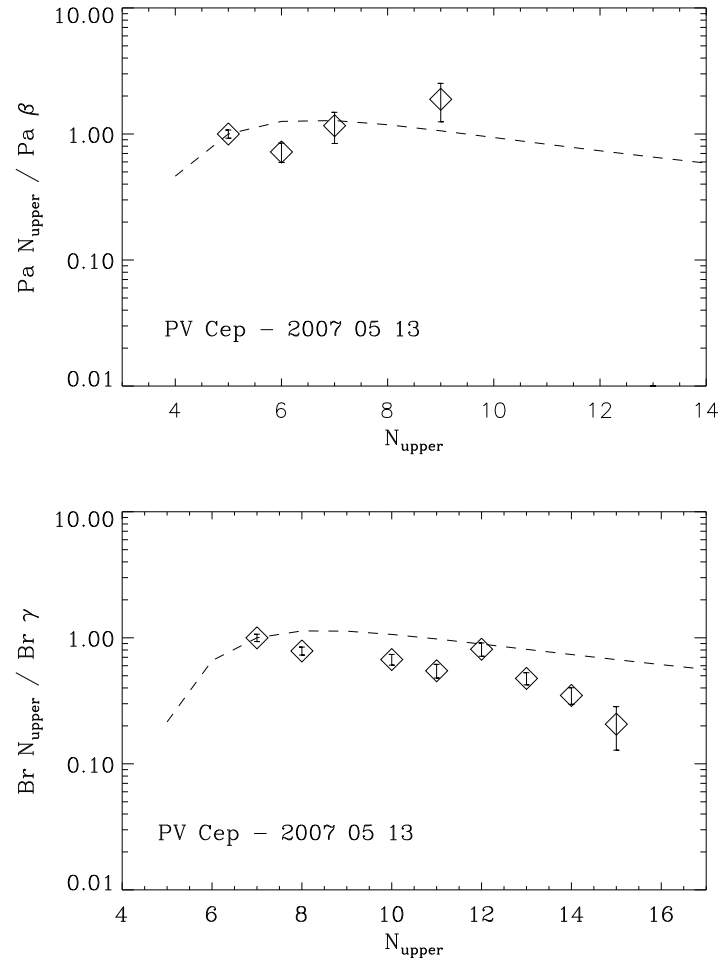


Fig. 13.— As Figure 11 for PV Cep.

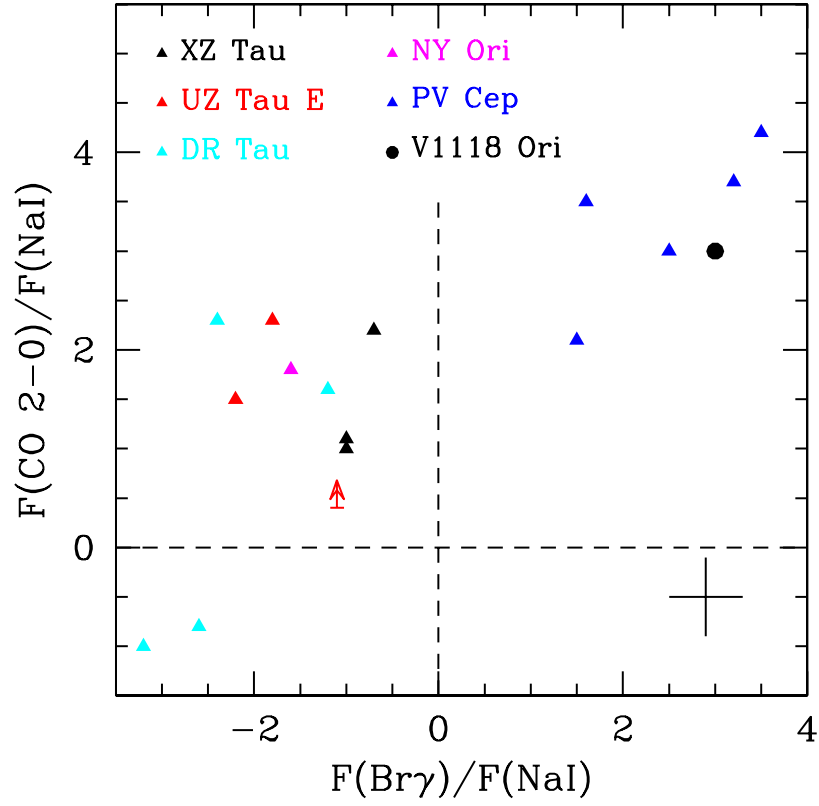


Fig. 14.— Observed ratios CO 2-0/NaI vs Br $\gamma$ /NaI. Dashed lines delimit the loci where the line ratios are positive or negative. The cross on the bottom right corner represents the typical error, obtained by propagating the average uncertainty of the individual line fluxes.

Table 1. EXOrs observed parameters.

Target	Dist.	$A_V$	$L_{bol}$	SpT	$V_{max}$	$V_{min}$	outf.	location	binary	Ref.
	(pc)	(mag)	( $L_{\odot}$ )		(mag)					
XZ Tau	140	3:	4.2 - 10.7	M3	10.4	16.6	Y	L1551	Y (0.30)	1,2,3,4,5,6
UZ Tau E	140	1.49	1.7	M1,3	11.7	15.0		B19	Y (0.34)	1,3
VY Tau	140	0.85	0.75	M0V	9.0	15.3		L1536	Y (0.66)	1,3,7
DR Tau	140	1.7-2.1	1.05-5.0	K7-M0	10.5	16.0		L1558	N	1,3,8,9
V1118 Ori	414	0-2	1.4-25.4	M1e	14.2	17.5	N	ONC	Y (0.18)	1,10,11,12
NY Ori	414	0.3		??	14.5	17.5		ONC	N	1,13,14
V1143 Ori	460			M	13	19		L1640	-	1
PV Cep	500	0.4-5	100	A5e	11.1	18.0	Y	L1158	-	1,15,16

Note. — References to the Table: (1) SIMBAD Astronomical Database (<http://simbad.u-strasbg.fr/simbad>); (2) Coffey, Downes & Ray 2004; (3) Herbig & Bell 1988; (4) Carr 1990; (5) Evans II et al. 1987; (6) Beck et al. 2008; (7) Herbig 1990; (8) Cohen & Kuhl 1979; (9) Kenyon et al. 1994; (10) Lorenzetti et al. (2006) - Paper I; (11) Reipurth et al. 2007; (12) Menten et al. 2007; (13) Breger, Gherz & Hackwell 1981; (14) Köhler et al. 2006; (15) Cohen et al. 1981; (16) van Citters & Smith 1989.

Table 2. Log of our observations: date on which spectra have been taken, near-IR magnitudes at that epoch and references to literature near-IR spectroscopic data.

Target	Date	J	H	K	Status <sup>a</sup>	Ref. to near-IR spectroscopy
		(mag)				
XZ Tau	2007 Mar 08	9.21	8.14	7.34	H	near- (1); Pa $\beta$ , Br $\gamma$ (2); Br $\gamma$ , Br $\alpha$ (3);
	2007 Oct 08	8.93	7.91	7.25	Hr	2-4 $\mu$ m (4); Br $\gamma$ , H <sub>2</sub> (5); Pa $\beta$ , Br $\gamma$ (6);
	2008 Mar 28	8.78	7.68	6.89	Hr	CO bands abs.(7); HeI, Pa $\gamma$ (8); extended H <sub>2</sub> emission (9).
UZ Tau E	2007 Mar 12	8.57	7.62	7.04	H	near- (10); HeI, Pa $\gamma$ (8)
	2007 Oct 11	8.62	7.75	7.22	Hd	
	2008 Mar 30	9.15	8.21	7.59	Hd	
VY Tau	2007 Mar 14	10.00	9.25	8.96	H	Pa $\beta$ (2); near- (1),(11); HeI, Pa $\gamma$ (8)
	2007 Oct 11	10.02	9.23	8.89	H	
	2008 Mar 30	9.99	9.21	8.91	H	
DR Tau	2007 Mar 13	8.68	7.57	6.52	I	near-(1); Pa $\beta$ , Br $\gamma$ (2); HeI (12);
	2007 Oct 08	8.83	7.70	6.76	I	Pa $\beta$ , Br $\gamma$ (6),(13); H <sub>2</sub> rot.
	2007 Nov 03	8.72	7.60	6.63	I	
	2008 Mar 28	8.76	7.66	6.70	I	
V1118 Ori	2005 Sep 11	11.23	10.45	9.85	H	near-, CO bands em.(14)/abs (17)
	2006 Sep 23	12.54	11.51	10.74	L	
NY Ori	2007 Mar 15	10.10	9.14	8.36		
	2007 Oct 14	10.01	9.02	8.27		
	2007 Oct 15	9.97	9.06	8.27		
	2007 Oct 24	10.22	9.18	8.34		
	2008 Mar 29	9.96	8.85	8.17		
V1143 Ori	2007 Mar 17	-	-	-		
	2007 Oct 15	12.65	11.88	11.62	I	
PV Cep	2007 May 13	11.52	9.33	7.54	L	Br $\gamma$ , H <sub>2</sub> (5); CO (7); [FeII] (15);
	2007 Oct 15	11.53	9.13	7.27	Lr	2-4 $\mu$ m (4)(16)
	2007 Oct 27	11.14	8.88	7.11	Lr	
	2008 Apr 01	10.09	8.12	6.54	Hr	
	2008 Apr 12	10.14	8.13	6.57	H	
	2008 Jun 10	11.96	9.36	7.38	Ld	
	2008 Jun 18	12.34	9.74	7.73	Ld	

Note. — References to the Table: (1) Folha & Emerson 1999; (2) Folha & Emerson 2001; (3) Evans et al. 1987; (4) Sato et al. 1990; (5) Carr 1990; (6) Giovanardi et al. 1991; (7) Biscaya et al. 1997; (8) Edwards et al. 2006; (9) Beck et al. 2008; (10) Elias 1978; (11) Greene & Lada 1996; (12) Edwards et al.

2003; (13) Muzerolle, Hartmann & Calvet 1998; (14) Paper I; (15) Hamann et al. 1994; (16) van Citters & Smith 1989; (17) Paper II.

<sup>a</sup> H = high, I = intermediate, L = low, r = rising, d = declining

Table 3. Line emission fluxes of XZ Tau.

$\lambda_{vac}$	Ident.	F $\pm$ $\Delta$ F	EW	F $\pm$ $\Delta$ F	EW	F $\pm$ $\Delta$ F	EW
( $\mu$ m)		07/Mar/08		07/Oct/08		08/Mar/28	
0.923	Pa9	< 11	-	< 6	-	-	-
0.955	Pa8	-	-	$3.5 \pm 1$	-5	$2.1 \pm 0.4$	-3
1.005	Pa $\delta$	$4 \pm 1$	-7	$5 \pm 1$	-7	$1.8 \pm 0.4$	-2
1.094	Pa $\gamma$	$4 \pm 2^*$	-8	$3.5 \pm 1$	-4	$8 \pm 4^*$	-8
1.117	?	-	-	$4 \pm 1$	-5	-	-
1.288	Pa $\beta$	$6 \pm 1$	-10	$6 \pm 2$	-7	$6 \pm 1$	-7
1.328	?	$3.2 \pm 0.6$	-5	$3.4 \pm 0.6$	-4	$1.8 \pm 0.6$	-2
2.166	Br $\gamma$	$2.4 \pm 0.2$	-4	$2.5 \pm 0.2$	-4	$1.6 \pm 0.4$	-2
2.208	NaI	$-2.5 \pm 0.6$	+4	$-2.5 \pm 0.6$	+4	$-2.4 \pm 0.6$	+4
2.267	CaI	$-2.6 \pm 0.6$	+5	$-1.2 \pm 0.6^*$	+2	<1.8	-
2.293	CO 2-0	$-2.5 \pm 0.6$	+5	$-2.7 \pm 0.6$	+5	$-5.3 \pm 0.4$	+8
2.323	CO 3-1	-	-	-	-	$-4.4 \pm 0.4$	+7

Note. — Fluxes marked with an asterisk are those derived at a  $2 < S/N < 3$  level; they will not be used in the following analysis.

- Fluxes and errors are given in units of  $10^{-13} \text{erg s}^{-1} \text{cm}^{-2}$ , while EW are expressed in ( $\text{\AA}$ )

- The values of  $\lambda_{oss}$  are not given since their difference with the  $\lambda_{vac}$  ones are always lesser than the spectral resolution element.

Table 4. Line emission fluxes of UZ Tau E.

$\lambda_{vac}$	Ident.	F $\pm$ $\Delta$ F	EW	F $\pm$ $\Delta$ F	EW	F $\pm$ $\Delta$ F	EW
( $\mu$ m)		07/Mar/12		07/Oct/11		08/Mar/30	
0.855	Pa15	9 $\pm$ 3	-19	-	-	-	-
0.867	Pa13	6 $\pm$ 2	-12	-	-	-	-
0.902	Pa10	3 $\pm$ 1	-7	-	-	-	-
0.923	Pa9	6 $\pm$ 1	-16	-	-	-	-
0.955	Pa8	6 $\pm$ 1	-10	6 $\pm$ 1	-5	15 $\pm$ 1	-10
1.005	Pa $\delta$	5 $\pm$ 1	-7	6 $\pm$ 1	-5	-	-
1.094	Pa $\gamma$	9 $\pm$ 1	-11	9 $\pm$ 1	-7	6 $\pm$ 1	-4
1.169	?	4 $\pm$ 1	-4	5 $\pm$ 1	-5	-	-
1.282	Pa $\beta$	11.4 $\pm$ 0.8	-13	10.4 $\pm$ 0.8	-10	10 $\pm$ 1	-8
1.328	?	5 $\pm$ 1	-5	3 $\pm$ 1	-3	3 $\pm$ 1	-3
1.491	Br27	4 $\pm$ 2*	-5	-	-	-	-
1.588	Br14	4 $\pm$ 2*	-4	-	-	-	-
1.611	Br13	4 $\pm$ 2*	-5	-	-	-	-
1.641	Br12	4 $\pm$ 2*	-5	4 $\pm$ 2*	-5	-	-
1.681	Br11	4 $\pm$ 2*	-4	-	-	-	-
1.694	?	4 $\pm$ 2*	-4	-	-	-	-
1.737	Br10	6 $\pm$ 3*	-7	-	-	-	-
2.166	Br $\gamma$	3.3 $\pm$ 0.8	-6	5.2 $\pm$ 0.8	-9	4 $\pm$ 1	-6
2.208	NaI	-1.8 $\pm$ 0.8*	+3	-2.4 $\pm$ 0.8	+4	-3.7 $\pm$ 0.8	+6
2.267	CaI	-2.4 $\pm$ 0.8	+3	-2.6 $\pm$ 0.8	+5	< 2.4	-
2.293	CO 2-0	-4.2 $\pm$ 0.8	+6	-3.7 $\pm$ 0.8	+7	-1.5 $\pm$ 0.7*	+2
2.323	CO 3-1	-4.1 $\pm$ 0.8	+6	-	-	-	-

Note. — The same as in Table 3.

Table 5. Line emission fluxes of VY Tau.

$\lambda_{vac}$	Ident.	F $\pm$ $\Delta$ F	EW	F $\pm$ $\Delta$ F	EW	F $\pm$ $\Delta$ F	EW
( $\mu$ m)		07/Mar/14		07/Oct/11		08/Mar/30	
1.094	Pa $\gamma$	< 1.8	-	3 $\pm$ 1	-11	3.1 $\pm$ 0.9	-9
1.282	Pa $\beta$	1.9 $\pm$ 0.4	-6	1.7 $\pm$ 0.4	-6	1.9 $\pm$ 0.4	-6
1.327	?	1.1 $\pm$ 0.5*	-4	<1.2	-	1.5 $\pm$ 0.4	-6
2.166	Br $\gamma$	0.5 $\pm$ 0.2*	-7	< 0.9	-	0.7 $\pm$ 0.2	-6
2.208	NaI	-1.2 $\pm$ 0.5*	+10	< 1.8	-	-0.4 $\pm$ 0.2*	+2.5
2.267	CaI	< 1.5	-	-	-	-0.5 $\pm$ 0.2*	+4
2.293	CO 2-0	-0.8 $\pm$ 0.5*	+7	-2.0 $\pm$ 0.5	+19	-0.6 $\pm$ 0.3*	+5

Note. — The same as in Table 3. Upper limits are given as  $3\sigma$  values.



Table 6. Line emission fluxes of DR Tau.

$\lambda_{vac}$	Ident.	F $\pm$ $\Delta$ F	EW	F $\pm$ $\Delta$ F	EW	F $\pm$ $\Delta$ F	EW	F $\pm$ $\Delta$ F	EW
( $\mu$ m)		07/Mar/13		07/Oct/08		07/Nov/03		08/Mar/28	
0.847	Pa17	-	-	-	-	$13 \pm 1$	-9	-	-
0.855	Pa15	$67 \pm 0.8$	-39	$50 \pm 1$	-67	$36 \pm 1$	-37	$75 \pm 1$	-73
0.867	Pa13	$29 \pm 0.8$	-16	$20 \pm 1$	-27	$34 \pm 1$	-25	$26 \pm 1$	-26
0.886	Pa11	$15 \pm 0.8$	-7	$5 \pm 1$	-7	$11 \pm 1$	-9	$16 \pm 1$	-16
0.902	Pa10	$15 \pm 0.8$	-8	$4 \pm 2^*$	-5	$15 \pm 2$	-13	$15 \pm 1$	-16
0.923	Pa9	$22 \pm 0.8$	-11	$9 \pm 1$	-12	$20 \pm 1$	-16	$16 \pm 1$	-17
0.955	Pa8	$21 \pm 0.8$	-14	$9 \pm 1$	-11	$21 \pm 1$	-17	$11.0 \pm 0.5$	-12
1.005	Pa $\delta$	$21 \pm 0.8$	-13	$12 \pm 1$	-15	$22 \pm 1$	-18	$13.4 \pm 0.5$	-13
1.070	?	$4.4 \pm 0.8$	-4	$3 \pm 1$	-4	$7 \pm 1$	-6	$3.7 \pm 0.5$	-4
1.094	Pa $\gamma$	$26 \pm 0.8$	-17	$18 \pm 2$	-22	$25 \pm 2$	-21	$20.0 \pm 0.5$	-20
1.117	CI?	$5 \pm 1$	-4	$5 \pm 1$	-6	-	-	$2 \pm 1^*$	-2
1.183	MgI	$2 \pm 1^*$	-1	$2 \pm 1^*$	-2	$2 \pm 1^*$	-2	$2 \pm 1^*$	-2
1.282	Pa $\beta$	$37 \pm 0.8$	-24	$24 \pm 2$	-26	$32 \pm 2$	-29	$30.0 \pm 0.5$	-31
1.328	?	$2.4 \pm 0.4$	-2	-	-	-	-	$3 \pm 1$	-4
1.491	Br27	$2.7 \pm 0.9$	-4	-	-	-	-	-	-
1.494	Br26	$2.1 \pm 0.2$	-4	-	-	-	-	$2.2 \pm 0.5$	-2
1.556	Br16	-	-	-	-	-	-	$2.2 \pm 0.5$	-2
1.570	Br15	-	-	-	-	-	-	$5.9 \pm 0.5$	-4
1.588	Br14	$5.5 \pm 0.6$	-6	$3.1 \pm 0.6$	-3	$7.7 \pm 0.6$	-6	$5.9 \pm 0.5$	-5
1.611	Br13	$6.9 \pm 0.6$	-7	$3.9 \pm 0.6$	-4	$4.7 \pm 0.6$	-4	$3.4 \pm 0.5$	-3
1.641	Br12	$6.8 \pm 0.6$	-7	$2.7 \pm 0.6$	-3	$7.3 \pm 0.6$	-6	$3.5 \pm 0.5$	-3
1.681	Br11	$4.8 \pm 0.6$	-2	$4.0 \pm 0.6$	-3	$7.2 \pm 0.6$	-6	$8.5 \pm 0.5$	-7
1.737	Br10	$6.6 \pm 0.6$	-7	$4.5 \pm 0.6$	-3	$8.2 \pm 0.6$	-7	$8.1 \pm 0.5$	-7
1.745	HeI ?	$7.1 \pm 0.6$	-7	$2.2 \pm 0.6$	-2	$3.4 \pm 0.6$	-3	-	-
1.945	Br $\delta$	$15 \pm 5$	-13	$16 \pm 5$	-16	$9.8 \pm 0.5$	-10	$14.0 \pm 0.5$	-19
2.059	HeI ?	$2.9 \pm 0.6$	-3	$2.4 \pm 0.6$	-2	$2.1 \pm 0.6$	-2	-	-
2.166	Br $\gamma$	$10 \pm 1$	-8	$6.2 \pm 0.6$	-6	$7.5 \pm 0.6$	-7	$7 \pm 1$	-6
2.208	NaI	$-3.1 \pm 0.4$	+3	$-2.4 \pm 0.4$	+3	$-3.1 \pm 0.4$	+3	$-5.7 \pm 0.4$	+5
2.267	CaI	$-2.5 \pm 0.4$	+2	$-1.0 \pm 0.4^*$	+1	-	-	-	-
2.293	CO 2-0	$3 \pm 1$	-3	$2.0 \pm 0.6$	-2	$-7.1 \pm 0.6$	+7	$-9.4 \pm 0.6$	+9
2.323	CO 3-1	-	-	$2.4 \pm 0.6$	-3	$-7.2 \pm 0.6$	+7	$-7.8 \pm 0.6$	+7

Note. — The same as in Table 3.

Table 7. Line emission fluxes of NY Ori.

$\lambda_{vac}$	Ident.	F $\pm$ $\Delta$ F	EW	F $\pm$ $\Delta$ F	EW	F $\pm$ $\Delta$ F	EW	F $\pm$ $\Delta$ F	EW	F $\pm$ $\Delta$ F	EW
( $\mu$ m)		07/Mar/15		07/Oct/14		07/Oct/15		07/Oct/24		08/Mar/29	
1.005	Pa $\delta$	-	-	$1.9 \pm 0.5$	-6	$1.0 \pm 0.5^*$	-3	-	-	-	-
1.094	Pa $\gamma$	$2.5 \pm 0.5$	-8	$3.0 \pm 0.5$	-9	$1.5 \pm 0.5$	-5	$1.2 \pm 0.5^*$	-4	$1.7 \pm 0.5$	-5
1.282	Pa $\beta$	$3.2 \pm 0.5$	-11	$4.0 \pm 0.5$	-13	$2.5 \pm 0.5$	-8	$2.2 \pm 0.5$	-7	$3.3 \pm 0.5$	-10
2.166	Br $\gamma$	$1.5 \pm 0.4$	-7	$1.1 \pm 0.4^*$	-5	$0.8 \pm 0.4^*$	-3	$1.3 \pm 0.4$	-6	$< 0.6$	-
2.208	NaI	$< 0.6$	-	$-0.7 \pm 0.3^*$	+3	$-1.0 \pm 0.4^*$	+4	$-0.8 \pm 0.4^*$	+4	$-1.1 \pm 0.3$	+4.5
2.293	CO 2-0	$0.6 \pm 0.2$	-3	$-1.3 \pm 0.5^*$	+6	$-0.8 \pm 0.4^*$	+3	$< 1.2$	-	$-1.9 \pm 0.3$	+8
2.323	CO 3-1	$0.9 \pm 0.2$	-5	-	-	-	-	-	-	$-1.8 \pm 0.3$	+7

Note. — The same as in Table 3. Upper limits are given as  $3\sigma$  values.

Table 8. Line emission fluxes of V1143 Ori.

$\lambda_{vac}$	Ident.	F $\pm$ $\Delta$ F	EW	F $\pm$ $\Delta$ F	EW
( $\mu$ m)		07/Mar/17		07/Oct/15	
1.094	Pa $\gamma$	$< 0.3$	-	$0.4 \pm 0.2^*$	-13
1.282	Pa $\beta$	$< 0.3$	-	$< 0.3$	-
2.166	Br $\gamma$	$< 0.2$	-	$< 0.8$	-
2.208	NaI	$< 0.2$	-	$-1.5 \pm 0.3$	+1
2.293	CO 2-0	$-0.3 \pm 0.1$	+33	$< 0.4$	-
2.323	CO 3-1	$-0.3 \pm 0.1$	+29	-	-

Note. — The same as in Table 3. Upper limits are given as  $3\sigma$  values.

Table 9. Line emission fluxes of PV Cep.

$\lambda_{vac}$	Ident.	F $\pm$ $\Delta$ F	EW	F $\pm$ $\Delta$ F	EW	F $\pm$ $\Delta$ F	EW	F $\pm$ $\Delta$ F	EW	F $\pm$ $\Delta$ F	EW
( $\mu$ m)		07/May/13		07/Oct/15		07/Oct/27		08/Apr/01		08/Apr/12	
0.836	Pa22	1.0 $\pm$ 0.1	-41	-	-	-	-	-	-	-	-
0.850	Pa16	3.5 $\pm$ 0.4	-138	2.8 $\pm$ 0.4	-176	< 4	-	4.0 $\pm$ 0.4	-53	1.0 $\pm$ 0.4*	-14
0.867	Pa13	1.5 $\pm$ 0.1	-68	2.4 $\pm$ 0.1	-136	3.2 $\pm$ 0.1	-254	2.5 $\pm$ 0.4	-32	2.0 $\pm$ 0.4	-28
0.923	Pa9	0.9 $\pm$ 0.3	-36	-	-	-	-	2.0 $\pm$ 0.3	-21	1.6 $\pm$ 0.3	-20
1.005	Pa $\delta$	1.1 $\pm$ 0.3	-33	0.6 $\pm$ 0.3*	-18	0.7 $\pm$ 0.3*	-18	1.6 $\pm$ 0.3	-13	1.2 $\pm$ 0.3	-11
1.070	?	1.0 $\pm$ 0.4*	-23	0.8 $\pm$ 0.4*	-15	1.1 $\pm$ 0.4*	-20	2.2 $\pm$ 0.4	-21	1.5 $\pm$ 0.4	-10
1.094	Pa $\gamma$	1.2 $\pm$ 0.2	-25	0.9 $\pm$ 0.2	-18	1.0 $\pm$ 0.2	-17	3.2 $\pm$ 0.2	-17	2.6 $\pm$ 0.2	-16
1.137	OI	0.8 $\pm$ 0.2	-16	0.8 $\pm$ 0.2	-15	0.5 $\pm$ 0.2*	-7	1.7 $\pm$ 0.2	-9	2.3 $\pm$ 0.2	-12
1.189	[PII]	-	-	0.8 $\pm$ 0.2	-11	-	-	-	-	-	-
1.205	?	1.3 $\pm$ 0.4	-19	0.8 $\pm$ 0.4*	-9	-	-	-	-	-	-
1.264	?	1.0 $\pm$ 0.4*	-13	0.8 $\pm$ 0.4*	-8	0.6 $\pm$ 0.2	-5	0.9 $\pm$ 0.3	-3	0.8 $\pm$ 0.2	-3
1.282	Pa $\beta$	3.8 $\pm$ 0.2	-48	3.7 $\pm$ 0.2	-40	3.5 $\pm$ 0.2	-28	5.3 $\pm$ 0.2	-16	6.1 $\pm$ 0.2	-20
1.504	Br23+MgI	1.7 $\pm$ 0.3	-9	1.9 $\pm$ 0.3	-7	2.5 $\pm$ 0.3	-10	5.6 $\pm$ 0.3	-8	3.8 $\pm$ 0.3	-6
1.570	Br15	0.8 $\pm$ 0.3*	-4	-	-	-	-	-	-	-	-
1.588	Br14	1.4 $\pm$ 0.2	-7	2.4 $\pm$ 0.2	-8	2.1 $\pm$ 0.2	-7	5.2 $\pm$ 0.2	-7	3.6 $\pm$ 0.2	-5
1.611	Br13	2.0 $\pm$ 0.4	-9	2.3 $\pm$ 0.4	-7	3.3 $\pm$ 0.4	-11	5.5 $\pm$ 0.4	-7	4.2 $\pm$ 0.4	-6
1.641	Br12	3.6 $\pm$ 0.4	-16	3.8 $\pm$ 0.4	-11	2.9 $\pm$ 0.4	-9	5.0 $\pm$ 0.4	-6	5.0 $\pm$ 0.4	-7
1.681	Br11	2.6 $\pm$ 0.3	-11	4.9 $\pm$ 0.3	-14	2.9 $\pm$ 0.3	-9	7.1 $\pm$ 0.3	-9	7.4 $\pm$ 0.3	-9
1.737	Br10	3.5 $\pm$ 0.3	-13	4.2 $\pm$ 0.3	-20	4.6 $\pm$ 0.3	-12	13.8 $\pm$ 0.3	-18	8.4 $\pm$ 0.3	-11
1.945	Br $\delta$	5.4 $\pm$ 0.3	-15	-	-	-	-	-	-	-	-
2.166	Br $\gamma$	8.5 $\pm$ 0.4	-17	7.8 $\pm$ 0.4	-11	7.3 $\pm$ 0.4	-11	8.3 $\pm$ 0.4	-7	9.6 $\pm$ 0.4	-8
2.208	NaI	2.6 $\pm$ 0.3	-5	5.3 $\pm$ 0.3	-7	2.1 $\pm$ 0.3	-3	5.1 $\pm$ 0.3	-4	3.9 $\pm$ 0.3	-3
2.293	CO 2-0	9.7 $\pm$ 0.7	-20	11.4 $\pm$ 0.7	-13	8.8 $\pm$ 0.7	-10	18.0 $\pm$ 0.7	-13	11.6 $\pm$ 0.7	-9
2.323	CO 3-1	12.8 $\pm$ 0.7	-20	10.9 $\pm$ 0.7	-12	10.3 $\pm$ 0.7	-10	20.2 $\pm$ 0.7	-15	11.7 $\pm$ 0.7	-8
		08/Jun/10		08/Jun/18							
1.005	Pa $\delta$	0.7 $\pm$ 0.2	-42	-	-						
1.094	Pa $\gamma$	0.5 $\pm$ 0.2*	-20	0.5 $\pm$ 0.2*	-19						
1.264	?	0.6 $\pm$ 0.2	-12	0.6 $\pm$ 0.2	-17						
1.282	Pa $\beta$	1.4 $\pm$ 0.2	-22	1.2 $\pm$ 0.2	-19						
2.166	Br $\gamma$	3.5 $\pm$ 0.4	-6	3.3 $\pm$ 0.6	-8						
2.208	NaI	< 1.3	-	< 1.4	-						
2.293	CO 2-0	1.3 $\pm$ 0.4	-2	2.6 $\pm$ 0.6	-5						
2.323	CO 3-1	1.8 $\pm$ 0.5	-3	1.8 $\pm$ 0.6	-3						

Note. — The same as in Table 3.

Table 10. EXor line flux variability in the near IR.

Source	Date	Pa $\gamma$	Pa $\beta$	Br $\gamma$	CO (2-0)	Status <sup>a</sup>	Ref
(10 <sup>-13</sup> erg s <sup>-1</sup> cm <sup>-2</sup> )							
XZ Tau	83 Nov	-	-	2.1 $\pm$ 0.5	-	H ?	2
	86 May - 87 Jan	-	-	0.42 $\pm$ 0.07	-	H ?	3
	88 Nov - 89 Jan	-	2.4 $\pm$ 0.4	0.9 $\pm$ 0.1	-		4
	<b>07 Mar</b>	<b>&lt; 0.6</b>	<b>6 <math>\pm</math> 1</b>	<b>2.4 <math>\pm</math> 0.2</b>	<b>-2.5 <math>\pm</math> 0.6</b>		<b>1</b>
	<b>07 Oct</b>	<b>3.5 <math>\pm</math> 1</b>	<b>6 <math>\pm</math> 2</b>	<b>2.5 <math>\pm</math> 0.2</b>	<b>-2.7 <math>\pm</math> 0.6</b>		<b>1</b>
	<b>08 Mar</b>	<b>&lt; 1.2</b>	<b>6 <math>\pm</math> 1</b>	<b>1.6 <math>\pm</math> 0.4</b>	<b>-5.3 <math>\pm</math> 0.4</b>		<b>1</b>
UZ Tau E	<b>07 Mar</b>	<b>9 <math>\pm</math> 1</b>	<b>10.9 <math>\pm</math> 0.8</b>	<b>4.5 <math>\pm</math> 0.8</b>	<b>-4.2 <math>\pm</math> 0.8</b>		<b>1</b>
	<b>07 Oct</b>	<b>9 <math>\pm</math> 1</b>	<b>10.4 <math>\pm</math> 0.8</b>	<b>5.2 <math>\pm</math> 0.8</b>	<b>-3.7 <math>\pm</math> 0.8</b>		<b>1</b>
	<b>08 Mar</b>	<b>6 <math>\pm</math> 1</b>	<b>10 <math>\pm</math> 1</b>	<b>4 <math>\pm</math> 1</b>	<b>&lt; 2.0</b>		<b>1</b>
VY Tau	<b>07 Mar</b>	<b>&lt; 1.8</b>	<b>1.9 <math>\pm</math> 0.4</b>	<b>&lt; 0.6</b>	<b>&lt; 1.0</b>		<b>1</b>
	<b>07 Oct</b>	<b>3 <math>\pm</math> 1</b>	<b>1.7 <math>\pm</math> 0.4</b>	<b>&lt; 0.9</b>	<b>-2.0 <math>\pm</math> 0.5</b>		<b>1</b>
	<b>08 Mar</b>	<b>3.1 <math>\pm</math> 0.9</b>	<b>1.9 <math>\pm</math> 0.4</b>	<b>0.7 <math>\pm</math> 0.2</b>	<b>&lt; 0.9</b>		<b>1</b>
DR Tau	88 Nov - 89 Jan	-	12 $\pm$ 1.2	3.2 $\pm$ 0.5	-	I ?	4
	<b>07 Mar</b>	<b>26 <math>\pm</math> 0.8</b>	<b>37 <math>\pm</math> 0.8</b>	<b>10 <math>\pm</math> 1</b>	<b>3 <math>\pm</math> 1</b>		<b>1</b>
	<b>07 Oct</b>	<b>18 <math>\pm</math> 2</b>	<b>24 <math>\pm</math> 2</b>	<b>6.2 <math>\pm</math> 0.6</b>	<b>2.0 <math>\pm</math> 0.6</b>		<b>1</b>
	<b>07 Nov</b>	<b>25 <math>\pm</math> 2</b>	<b>32 <math>\pm</math> 2</b>	<b>7.5 <math>\pm</math> 0.6</b>	<b>-7.1 <math>\pm</math> 0.6</b>		<b>1</b>
	<b>08 Mar</b>	<b>20.0 <math>\pm</math> 0.5</b>	<b>30.0 <math>\pm</math> 0.5</b>	<b>7 <math>\pm</math> 1</b>	<b>-9.4 <math>\pm</math> 0.6</b>		<b>1</b>
V1118 Ori	<b>05 Sep</b>	<b>2.5 <math>\pm</math> 0.2</b>	<b>4.1 <math>\pm</math> 0.1</b>	<b>1.2 <math>\pm</math> 0.2</b>	<b>1.2 <math>\pm</math> 0.4</b>	H	<b>5</b>
	<b>06 Sep</b>	<b>&lt; 0.4</b>	<b>&lt; 0.6</b>	<b>&lt; 0.2</b>	<b>-</b>		<b>6</b>
NY Ori	<b>07 Mar</b>	<b>2.5 <math>\pm</math> 0.5</b>	<b>3.2 <math>\pm</math> 0.5</b>	<b>1.5 <math>\pm</math> 0.4</b>	<b>0.6 <math>\pm</math> 0.2</b>		<b>1</b>
	<b>07 Oct</b>	<b>3 <math>\pm</math> 0.5</b>	<b>4.0 <math>\pm</math> 0.5</b>	<b>&lt; 1.2</b>	<b>&lt; 1.5</b>		<b>1</b>
	<b>07 Oct</b>	<b>1.5 <math>\pm</math> 0.5</b>	<b>2.5 <math>\pm</math> 0.5</b>	<b>&lt; 1.2</b>	<b>&lt; 1.2</b>		<b>1</b>
	<b>07 Oct</b>	<b>&lt; 1.5</b>	<b>2.2 <math>\pm</math> 0.5</b>	<b>1.3 <math>\pm</math> 0.4</b>	<b>&lt; 1.2</b>		<b>1</b>
	<b>08 Mar</b>	<b>1.7 <math>\pm</math> 0.5</b>	<b>3.3 <math>\pm</math> 0.5</b>	<b>&lt; 0.6</b>	<b>-1.9 <math>\pm</math> 0.3</b>		<b>1</b>
V1143 Ori	<b>07 Mar</b>	<b>&lt; 0.3</b>	<b>&lt; 0.3</b>	<b>&lt; 0.2</b>	<b>-0.3 <math>\pm</math> 0.1</b>		<b>1</b>
	<b>07 Oct</b>	<b>&lt; 0.6</b>	<b>&lt; 0.3</b>	<b>&lt; 0.8</b>	<b>&lt; 0.4</b>		<b>1</b>
PV Cep	86 Jul	-	-	0.44 $\pm$ 0.05	-		3
	86 Oct	-	-	0.80 $\pm$ 0.12	-		3
	<b>07 Mar</b>	<b>1.2 <math>\pm</math> 0.2</b>	<b>3.8 <math>\pm</math> 0.2</b>	<b>8.5 <math>\pm</math> 0.4</b>	<b>9.7 <math>\pm</math> 0.7</b>		<b>1</b>
	<b>07 Oct</b>	<b>0.9 <math>\pm</math> 0.2</b>	<b>3.7 <math>\pm</math> 0.2</b>	<b>7.8 <math>\pm</math> 0.4</b>	<b>11.4 <math>\pm</math> 0.7</b>		<b>1</b>
	<b>07 Oct</b>	<b>1.0 <math>\pm</math> 0.2</b>	<b>3.5 <math>\pm</math> 0.2</b>	<b>7.3 <math>\pm</math> 0.4</b>	<b>8.8 <math>\pm</math> 0.7</b>		<b>1</b>
	<b>08 Apr</b>	<b>3.2 <math>\pm</math> 0.2</b>	<b>5.3 <math>\pm</math> 0.2</b>	<b>8.3 <math>\pm</math> 0.4</b>	<b>18 <math>\pm</math> 0.7</b>		<b>1</b>
	<b>08 Apr</b>	<b>2.6 <math>\pm</math> 0.2</b>	<b>6.1 <math>\pm</math> 0.2</b>	<b>9.6 <math>\pm</math> 0.4</b>	<b>11.6 <math>\pm</math> 0.7</b>		<b>1</b>

Table 10—Continued

Source	Date	Pa $\gamma$	Pa $\beta$	Br $\gamma$	CO (2-0)	Status <sup>a</sup>	Ref
Equivalent Width (in Å)							
XZ Tau	02 Nov	-1.0	-	-	-		7
	<b>07 Mar</b>	-	<b>-10</b>	<b>-4</b>	<b>+5</b>		<b>1</b>
	<b>07 Oct</b>	<b>-4</b>	<b>-7</b>	<b>-4</b>	<b>+5</b>		<b>1</b>
	<b>08 Mar</b>	-	<b>-7</b>	<b>-2</b>	<b>+8</b>		<b>1</b>
UZ Tau E	02 Nov	-4.0	-		-	H ?	7
	<b>07 Mar</b>	<b>-11</b>	<b>-13</b>	<b>-6</b>	<b>+6</b>		<b>1</b>
	<b>07 Oct</b>	<b>-7</b>	<b>-10</b>	<b>-9</b>	<b>+7</b>		<b>1</b>
	<b>08 Mar</b>	<b>-4</b>	<b>-8</b>	<b>-6</b>	-		<b>1</b>
VY Tau	<b>07 Mar</b>	-	<b>-6</b>	-	-		<b>1</b>
	<b>07 Oct</b>	<b>-11</b>	<b>-6</b>	-	<b>+19</b>		<b>1</b>
	<b>08 Mar</b>	<b>-9</b>	<b>-6</b>	<b>-6</b>	-		<b>1</b>
DR Tau	98 Jan	-	-21.2	-7.3	-	I	8
	02 Nov	-12.3/-13.7	-	-	-		7
	<b>07 Mar</b>	<b>-17</b>	<b>-24</b>	<b>-8</b>	<b>-3</b>		<b>1</b>
	<b>07 Oct</b>	<b>-22</b>	<b>-26</b>	<b>-6</b>	<b>-2</b>		<b>1</b>
	<b>07 Nov</b>	<b>-21</b>	<b>-29</b>	<b>-7</b>	<b>+7</b>		<b>1</b>
	<b>08 Mar</b>	<b>-20</b>	<b>-31</b>	<b>-6</b>	<b>+9</b>		<b>1</b>
V1118 Ori	<b>05 Sep</b>	<b>-20</b>	<b>-40</b>	<b>-30</b>	<b>-30</b>		<b>5</b>
	<b>06 Sep</b>	-	-	-	-		<b>6</b>
NY Ori	<b>07 Mar</b>	<b>-8</b>	<b>-11</b>	<b>-7</b>	<b>-3</b>		<b>1</b>
	<b>07 Oct</b>	<b>-9</b>	<b>-13</b>	<b>-5</b>	-		<b>1</b>
	<b>07 Oct</b>	<b>-5</b>	<b>-8</b>	<b>-3</b>	-		<b>1</b>
	<b>07 Oct</b>	-	<b>-7</b>	<b>-6</b>	-		<b>1</b>
	<b>08 Mar</b>	<b>-5</b>	<b>-10</b>	-	<b>+8</b>		<b>1</b>
V1143 Ori	<b>07 Mar</b>	-	-	-	<b>+33</b>		<b>1</b>
	<b>07 Oct</b>	-	-	-	-		<b>1</b>
PV Cep	86	-	-	-	< -3.1		3
	94 Jun	-	-	-	-4.4		9
	95 Jan	-	-18.2	-2.4	-		10
	<b>07 Mar</b>	<b>-25</b>	<b>-48</b>	<b>-17</b>	<b>-20</b>		<b>1</b>
	<b>07 Oct</b>	<b>-18</b>	<b>-40</b>	<b>-11</b>	<b>-13</b>		<b>1</b>
	<b>07 Oct</b>	<b>-17</b>	<b>-28</b>	<b>-11</b>	<b>-10</b>		<b>1</b>
	<b>08 Apr</b>	<b>-17</b>	<b>-16</b>	<b>-7</b>	<b>-13</b>		<b>1</b>
	<b>08 Apr</b>	<b>-16</b>	<b>-20</b>	<b>-8</b>	<b>-9</b>		<b>1</b>

Note. — References to the Table: **(1) Present paper**; (2) Evans et al. 1987; (3) Carr 1990; (4) Giovanardi et al. 1991; (5) Paper I; (6) Paper II; (7) Edwards et al. 2006; (8) Muzerolle, Hartmann & Calvet 1998; (9) Biscaya et al. 1997; (10) Greene & Lada 1996.

<sup>a</sup> H = high, I = intermediate, L = low, r = rising, d = declining

Table 11. EXor wind parameters.

Source	Date	$A_V$	$R_{out}$	T	$\text{Pa}\beta$	$\text{Br}\gamma$	$\text{Pa}\beta/\text{Br}\gamma$	$\text{Pa}\beta/\text{Br}\gamma$	$\dot{M}_{wind}$
		(mag)	( $R_*$ )	(K)	(mod/obs)		(mod)	(obs)	( $10^{-7} \text{ M}_\odot \text{ yr}^{-1}$ )
UZ Tau E	07 Mar 12	1.5	3.0	6000	1.2	0.9	4.4	3.3	0.1
	07 Oct 11	1.5	3.0	6000	1.4	0.9	4.4	2.5	0.1
DR Tau	07 Mar 13	1.9	3.0	7400	1.0	1.0	3.6	3.7	0.6
	07 Oct 08	1.9	3.0	6400	1.0	1.0	3.8	3.9	0.3
	07 Nov 03	1.9	3.0	6400	1.0	1.3	3.1	4.3	0.6
	08 Mar 28	1.9	3.0	8000	1.0	1.0	4.1	4.3	0.4
	05 Sep 10	0	5.0	8000	1.1	1.1	3.6	3.4	0.4
V1118 Ori	07 May 13	11	5.0	6000	1.0	0.7	0.6	2.3	9.7
	07 Oct 15	13	7.0	6000	1.0	0.6	0.7	3.3	5.1
	07 Oct 27	11	20	6000	1.0	0.4	1.3	2.5	2.0
	08 Apr 01	9	4.5	6000	1.0	0.8	0.8	2.5	21
	08 Apr 12	9	4.5	6000	1.0	0.6	0.9	2.5	6.7
	08 Jun 10	14.5	3.5	7000	1.0	1.0	0.4	3.5	22
	08 Jun 18	14.5	4.0	6000	1.0	0.9	0.4	3.2	8.2

Table 12. EXor accretion parameters.

Source	Date	$\Delta L_{JHK}$	$A_V$	$L_{acc}(\text{Pa}\beta)$	$L_{acc}(\text{Br}\gamma)$	$\dot{M}_{acc}$
		( $L_\odot$ )	(mag)	( $L_\odot$ )	( $L_\odot$ )	( $10^{-7} \text{ M}_\odot \text{ yr}^{-1}$ )
UZ Tau E	07 Mar 12	-	1.5	0.5	1.0	1-3
	07 Oct 11	- 0.1	1.5	0.5	1.2	1-3
DR Tau	07 Mar 13	-	1.9	2.3	2.9	7-9
	07 Oct 08	- 0.2	1.9	0.9	1.3	3-4
	07 Nov 03	- 0.1	1.9	2.0	2.0	6
	08 Mar 28	- 0.1	1.9	1.8	1.9	4
	05 Sep 10	-	0	1.5	2.5	4-7
V1118 Ori	06 Sep 23	- 0.4	2.5	-	-	-
	07 May 13	-	11	41.7	182	25-100
PV Cep	07 Oct 15	+ 1.3	13	72.4	219	47-130
	07 Oct 27	+ 2.4	11	38.0	158	23-95
	08 Apr 01	+ 8.0	9	34.7	147	21-88
	08 Apr 12	+ 7.6	9	40.7	170	24-100
	08 Jun 10	+ 0.6	14.5	37.0	91.6	22-55
	08 Jun 18	- 0.9	14.5	31.5	81.3	19-49

Table 13. Parameters of the candidate EXor’s.

Source	Status	Near-IR spect.	P <sub>Cyg</sub>	B or R while brightening	Ref.
SVS 13	rising	increasing CO em. HI, NaI, CO, H <sub>2</sub> , [FeII] CO (but no EW) variability	PC H $\alpha$ , HH + CO narrow line	blueing	1,2,3 4,5,6 7
L1415 IRS	rising	no IR spectrum	PC H $\alpha$ , HH		8
V1647 Ori	outburst	Br $\gamma$ , NaI, CO	PC H $\alpha$	blueing	9,10
	outburst	recomb., ionic, CO	PC Paschen, HeI		11
	fading	recomb., ionic, CO	PC absent		12
	fading	CO rovibrational	–		13
	quiescent	line em. steady decrease	PC absent		14
	quiescent	CO abs., HI, He fading	–		15
ISO Cha I 192	rising	recomb., ionic, CO	CO outflow	blueing	16
OO Ser	rising	featureless, rising cont.	–		17
	fading	faint CO bandhead abs.	–		18
	fading	featureless, rising cont.	–		19
EC 53	fading	no IR spectrum	–	blueing	17
	variab.	no IR spectrum	–	no color var.	18
		abs. features	–		20
GM Cep	rising	no IR spectrum	PC H $\alpha$	random color var.	21

Note. — (1) Eislöffel et al. 1991; (2) Liseau, Lorenzetti & Molinari 1992; (3) Carr 1990; (4) Davis et al. 2006; (5) Takami et al. 2006 (and references therein); (6) Davis et al. 2002; (7) Biscaya et al. 1997; (8) Stecklum, Melnikov & Meusinger 2007; (9) Reipurth & Aspin 2004; (10) Walter et al. 2004; (11) Vacca, Cushing & Simon 2004; (12) Gibb et al. 2006; (13) Brittain et al. 2007; (14) Acosta-Pulido et al. 2007; (15) Aspin, Beck & Reipurth 2008; (16) Gómez & Mardones 2003; (17) Hodapp et al. 1996; (18) Hodapp 1999; (19) Kóspál et al. 2007; (20) Doppmann et al. 2005; (21) Sicilia-Aguilar et al. 2007.

<sup>a</sup> PC = P<sub>Cyg</sub> profile; IPC = inverse P<sub>Cyg</sub> profile; EW = Equivalent Width.